

Asymptotic security analysis of discrete-modulated continuous-variable quantum key distribution

Jie Lin, Twesh Upadhyaya, and Norbert Lütkenhaus

*Institute for Quantum Computing and Department of Physics and Astronomy,
University of Waterloo, Waterloo, Ontario, Canada N2L 3G1*

(Dated: May 28, 2019)

Continuous-variable quantum key distribution (CV-QKD) protocols with discrete modulation are interesting due to their experimental simplicity, but their security analysis is less advanced than that of Gaussian modulation schemes. We analyze the security of two variants of CV-QKD protocol with quaternary modulation against collective attacks in the asymptotic limit. Our security analysis is based on the numerical optimization of the asymptotic key rate formula with a photon number cutoff assumption that truncates the dimension of the system. When the cutoff photon number is chosen to be sufficiently large, our results do not depend on the specific choice of cutoff. Our analysis shows that this protocol can achieve much higher key rates over long distances compared with binary and ternary modulation schemes and yield key rates comparable to Gaussian modulation schemes. Furthermore, our security analysis method allows us to evaluate variations of the discrete-modulated protocols, including direct and reverse reconciliation, and also postselection strategies. We also demonstrate that postselection in combination with reverse reconciliation can improve the key rates.

I. INTRODUCTION

Quantum key distribution (QKD) [1, 2] is an important cryptographic primitive in the era of quantum technology since it enables two honest parties, traditionally known as Alice and Bob, to establish information-theoretically secure keys against any eavesdropper (Eve) who is bound by the laws of quantum mechanics. By now, there are plenty of QKD protocols (see [3] for a review), which can be categorized into two families according to their detection technology: discrete variable (DV) and continuous variable (CV). DV-QKD protocols like BB84 [1] are realized by encoding the information into qubit-like degree of freedom of photons, such as polarization and time-bin, and by measuring with single-photon detectors. DV-QKD enjoys a great success in experimental implementations and corresponding security analyses, and can currently reach longer distances than CV-QKD. However, CV-QKD (e.g. see Refs. [4–6]) uses detection technology that is widely used in modern optical (classical) communication methods, which turns those classical methods and CV-QKD apparatus into nearly identical devices. This gives CV-QKD a competitive edge for the large-scale deployment in quantum-secured networks.

A main security proof technique for CV-QKD is the optimality of Gaussian attacks [7, 8] for protocols with Gaussian modulation. In fact, security proofs are quite mature for CV-QKD with Gaussian modulation (see [9] for a review). This type of protocols puts a lot of demands on the modulation devices and classical error correction protocols. In addition, the effect of finite constellation needs to be taken into account carefully [10, 11]. In probing quantumness of devices using coherent states, we noticed that even a small number of coherent states has the same quantumness verification power as a Gaussian modulation of states [12]. We thus expect that a discrete-modulated CV-QKD protocol will approach the

performance of Gaussian modulated CV-QKD with just a few different modulation amplitudes. However, the corresponding security proof is more involved due to missing analytical tools. The binary [13] and ternary modulation schemes [14] have been proved secure against collective attacks. Unfortunately, the key rates obtained are not tight and the proof technique is not expected to be generalizable to discrete modulation schemes with more states. Moreover, these proofs are valid only if the receiver observes a Gaussian distribution of outcomes. For the quaternary modulation scheme, also known as quadrature phase-shift keying scheme, its security was previously analyzed under the assumption of linear bosonic channels [15] or Gaussian attacks [16], which restricts Eve's ability. Also the key rate obtained in Ref. [15] is not expected to be tight. Recently, there is a security analysis [17] of the quaternary modulation scheme with heterodyne detection. This security analysis uses a reduction to the Gaussian optimality proof method and applies a semidefinite program (SDP) technique with a photon number cutoff assumption. As we show in our contribution, one can improve their key rates. Furthermore, our approach can be extended to variants of the protocol using homodyne measurements. Our approach and proof technique will also allow postselection [18, 19], which is commonly done for the classical telecommunication protocols and DV-QKD protocols but not considered in Ref. [17] due to the proof technique.

In this work, we consider two variants of the quadrature phase-shift keying modulation scheme: one with homodyne detection and the other with heterodyne detection. For these two variants, we analyze the security against collective attacks in the asymptotic limit. Remarkably, compared with the similar heterodyne scheme considered in Ref. [17], we obtain quite higher key rates. We want to point out that this result can be further improved by a suitable choice of key map and error-

correction protocol. Since our method does not invoke the argument about optimality of Gaussian attacks, we also investigate the effects of postselection in which case Gaussian attacks are not known to be optimal. Previously, postselection was considered for discrete modulation scheme under a restricted class of attacks [16, 20]. From our results, we observe that postselection can improve the key rates under collective attacks. We remark that our security proof method works for both direct reconciliation and reverse reconciliation protocols. However, we focus on reverse reconciliation in this work since reverse reconciliation is known to have better performance than the direct reconciliation in terms of transmission distances. For our security analysis, we rely on the numerical methods developed in Refs. [21, 22] and we use the version of Ref. [22] to prove the security against collective attacks in the asymptotic limit. In order to perform such an optimization numerically, we impose the same photon number cutoff assumption considered in Ref. [17]. Although ultimately one would like to prove the security without this assumption, this assumption is reasonable because we notice that when the cutoff photon number is much larger than the mean photon number, we numerically verify that our key rate results do not depend on the choice of cutoff. We leave it as the future work to remove this assumption. It is also interesting to point out that our approach can be easily generalized to other discrete modulation schemes beyond four coherent states.

The rest of the paper is outlined as follows. In Sec. II, we present two variants of the protocol: protocol 1 uses the homodyne detection and only uses two out of four states to generate keys; protocol 2 uses the heterodyne detection and encodes 2-bit information in each round. In Sec. III, we first review the relevant numerical approach used for this work, discuss the photon number cutoff assumption and then present the specific setup of the optimization problems for those two protocols, such as choices of constraints, the postprocessing map and the pinching map related to the key map. We then perform simulations and show the simulation results in Sec. IV. Finally, we summarize the results and provides insights for the future direction in Sec. V. We discuss some technical details in the appendixes.

II. DESCRIPTION OF PROTOCOLS

In the following description, let $[N]$ denote the set of positive integers from 1 to N . When Greek letters α, γ are put in the bra-ket notation, we refer to coherent states with amplitude α or γ .

A. Protocol 1: with homodyne detection

- (1). State preparation. For each round $k \in [N]$ (where N is sufficiently large), according to the

probability distribution $(\frac{p_A}{2}, \frac{p_A}{2}, \frac{1-p_A}{2}, \frac{1-p_A}{2})$, Alice prepares a coherent state $|\psi_k\rangle$ from the set $\{|\alpha\rangle, |-\alpha\rangle, |i\alpha\rangle, |-i\alpha\rangle\}$, where $\alpha \in \mathbb{R}$ is predetermined. Alice sends this state to Bob through an insecure quantum channel.

- (2). Measurement. After receiving Alice's state, Bob performs the homodyne measurement on the state. Bob generates a random bit b_k according to the probability distribution $(p_B, 1 - p_B)$. If $b_k = 0$, he measures the q quadrature and if $b_k = 1$, he measures the p quadrature. He obtains the measurement outcome $y_k \in \mathbb{R}$.
- (3). Announcement and sifting. After N rounds of first two steps, Alice and Bob communicate via the authenticated classical channel to partition all the rounds $[N]$ into four subsets defined as

$$\begin{aligned} \mathcal{I}_{qq} &= \{k \in [N] : |\psi_k\rangle \in \{|\alpha\rangle, |-\alpha\rangle\}, b_k = 0\}, \\ \mathcal{I}_{qp} &= \{k \in [N] : |\psi_k\rangle \in \{|\alpha\rangle, |-\alpha\rangle\}, b_k = 1\}, \\ \mathcal{I}_{pq} &= \{k \in [N] : |\psi_k\rangle \in \{|i\alpha\rangle, |-i\alpha\rangle\}, b_k = 0\}, \\ \mathcal{I}_{pp} &= \{k \in [N] : |\psi_k\rangle \in \{|i\alpha\rangle, |-i\alpha\rangle\}, b_k = 1\}. \end{aligned} \quad (1)$$

Then Alice and Bob randomly select a small test subset $\mathcal{I}_{qq,\text{test}} \subset \mathcal{I}_{qq}$. This allows them to define \mathcal{I}_{key} as the subset of \mathcal{I}_{qq} after removing $\mathcal{I}_{qq,\text{test}}$ and to define $\mathcal{I}_{\text{test}} = \mathcal{I}_{qq,\text{test}} \cup \mathcal{I}_{qp} \cup \mathcal{I}_{pq} \cup \mathcal{I}_{pp}$. Let m denote the size of the index set \mathcal{I}_{key} and let f be a bijective function from $[m] = \{1, 2, \dots, m\}$ to \mathcal{I}_{key} . After sifting, Alice sets her string $\mathbf{X} = (x_1, x_2, \dots, x_m)$ according to the rule

$$\forall j \in [m], x_j = \begin{cases} 0 & \text{if } |\psi_{f(j)}\rangle = |\alpha\rangle, \\ 1 & \text{if } |\psi_{f(j)}\rangle = |-\alpha\rangle. \end{cases} \quad (2)$$

- (4). Parameter estimation. Alice and Bob perform parameter estimation by disclosing all the information in the rounds indexed by the test set $\mathcal{I}_{\text{test}}$. To perform such an analysis, they process the data by computing quantities like the first and second moments of q and p quadratures conditioned on each of four states that Alice sends. These quantities allow them to constrain their joint state ρ_{AB} . They then calculate the secret key rate according to the optimization problem presented in Eq. (16). If their analysis shows that no secret keys can be generated, then they abort the protocol. Otherwise, they proceed.
- (5). Reverse reconciliation key map. Bob performs a key map to obtain his raw key string. This key map discretizes his measurement outcome y_k to an element in the set $\{0, 1, \perp\}$ for each $k \in \mathcal{I}_{\text{key}}$. For each $j \in [m]$, Bob sets z_j according to the rule

$$z_j = \begin{cases} 0 & \text{if } y_{f(j)} \in [\Delta_c, \infty), \\ 1 & \text{if } y_{f(j)} \in (-\infty, -\Delta_c], \\ \perp & \text{if } y_{f(j)} \in (-\Delta_c, \Delta_c). \end{cases} \quad (3)$$

Note that $\Delta_c \geq 0$ is a parameter related to the postselection. A protocol without postselection can set $\Delta_c = 0$. At end of this process, Bob has a string $\mathbf{Z} = (z_1, z_2, \dots, z_m)$. In communication between Alice and Bob, positions with the symbol \perp are deleted from their strings. With a slight abuse of notation, we use \mathbf{X}, \mathbf{Z} to mean the strings after removing the positions related to \perp . \mathbf{Z} is called the raw key string.

- (6). Error correction and privacy amplification. Alice and Bob then apply a suitable error correction protocol and a privacy amplification protocol to generate a secret key.

Remark: In the description above, Alice and Bob essentially only use a subset of \mathcal{I}_{qq} to generate keys. For this specific setup, we consider asymmetric roles of these four states and asymmetric choice of quadrature measurements. In the asymptotic limit, we can set p_A and p_B arbitrarily close to 1 so that the sifting factor of the protocol is 1 (in the absence of postselection) [23]. In this sense, Alice's signal states $|i\alpha\rangle$ and $|-i\alpha\rangle$ and Bob's p quadrature measurement data are only used to probe eavesdropping activities. One needs to optimize p_A and p_B when the finite-size effects are taken into consideration. For another variant of this protocol, one may choose $p_A = p_B = \frac{1}{2}$ and allow Alice and Bob to generate keys from both \mathcal{I}_{qq} and \mathcal{I}_{pp} . Then the protocol would have $\frac{1}{2}$ sifting factor (in the absence of postselection). Since the essential idea of our security proof in the asymptotic limit is the same, we consider the asymmetric version to maximize the sifting factor in this work.

B. Protocol 2: with heterodyne detection

This variant differs from the protocol 1 in the steps (2), (3), (5).

- (1). State preparation. Like the protocol 1, Alice prepares one of those four signal states with an equal probability ($p_A = \frac{1}{2}$) and sends to Bob.
- (2'). Measurement. Upon receiving Alice's state, Bob performs the heterodyne measurement on the state, which can be described by a positive operator-valued measure (POVM) $\{E_\gamma = \frac{1}{\pi} |\gamma\rangle\langle\gamma| : \gamma \in \mathbb{C}\}$. After applying this POVM, he obtains the measurement outcome $y_k \in \mathbb{C}$.
- (3'). Announcement and sifting. After N rounds of first two steps, Alice and Bob determine a small subset $\mathcal{I}_{\text{test}} \subset [N]$. Rounds indexed by the set $\mathcal{I}_{\text{test}}$ are used for parameter estimation. They will use the remaining rounds indexed by $\mathcal{I}_{\text{key}} = [N]/\mathcal{I}_{\text{test}}$ to generate keys. Let m denote the size of the index set \mathcal{I}_{key} and let f be a bijective function from $[m]$ to \mathcal{I}_{key} . After sifting, Alice obtains her string $\mathbf{X} = (x_1, \dots, x_m)$ by the

following rule

$$\forall j \in [m], x_j = \begin{cases} 0 & \text{if } |\psi_{f(j)}\rangle = |\alpha\rangle, \\ 1 & \text{if } |\psi_{f(j)}\rangle = |i\alpha\rangle, \\ 2 & \text{if } |\psi_{f(j)}\rangle = |-\alpha\rangle, \\ 3 & \text{if } |\psi_{f(j)}\rangle = |-i\alpha\rangle. \end{cases} \quad (4)$$

- (4). Parameter estimation. As with the protocol 1, Alice and Bob perform parameter estimation to decide whether they abort the protocol.
- (5'). Reverse reconciliation key map. Bob performs a key map to obtain his raw key string. This key map discretizes his measurement outcome y_k to an element in the set $\{0, 1, 2, 3, \perp\}$ for each $k \in \mathcal{I}_{\text{key}}$. As $y_k \in \mathbb{C}$, we write $y_k = |y_k|e^{i\theta_k}$, where $\theta_k \in [-\frac{\pi}{4}, \frac{7\pi}{4})$. Bob sets each z_j of his key string $\mathbf{Z} = (z_1, \dots, z_m)$ according to the rule

$$z_j = \begin{cases} 0 & \text{if } \theta_{f(j)} \in [-\frac{\pi}{4} + \Delta_p, \frac{\pi}{4} - \Delta_p) \text{ and } |y_{f(j)}| \geq \Delta_a, \\ 1 & \text{if } \theta_{f(j)} \in [\frac{\pi}{4} + \Delta_p, \frac{3\pi}{4} - \Delta_p) \text{ and } |y_{f(j)}| \geq \Delta_a, \\ 2 & \text{if } \theta_{f(j)} \in [\frac{3\pi}{4} + \Delta_p, \frac{5\pi}{4} - \Delta_p) \text{ and } |y_{f(j)}| \geq \Delta_a, \\ 3 & \text{if } \theta_{f(j)} \in [\frac{5\pi}{4} + \Delta_p, \frac{7\pi}{4} - \Delta_p) \text{ and } |y_{f(j)}| \geq \Delta_a, \\ \perp & \text{if } \theta_{f(j)} \text{ and } |y_{f(j)}| \text{ are none of the above.} \end{cases} \quad (5)$$

$\Delta_a \geq 0$ and $\Delta_p \geq 0$ are two parameters related to postselection. A protocol without postselection can set $\Delta_a = \Delta_p = 0$. This key map is depicted in Fig. 1. Like the protocol 1, positions with the symbol \perp are deleted from their strings. Again, we use \mathbf{X}, \mathbf{Z} to mean the strings after removing the positions related to \perp . \mathbf{Z} is called the raw key string.

- (6). Error correction and privacy amplification. As with the protocol 1, they perform error correction and privacy amplification to generate a secret key.

Alice and Bob may decide to recast their strings to binary strings before or during the error correction step depending on their choice of error-correcting code. For the consistency of our presentation, we use the alphabet $\{0, 1, 2, 3\}$ in the following discussion.

III. SECURITY PROOF APPROACH

Our security proof applies the numerical key rate calculation framework developed in Refs. [21, 22], which allows us to calculate the secret key rate against collective attacks in the asymptotic limit. Specifically, we implement the approach in Ref. [22] to solve the key rate optimization problem in this work. We begin with reviewing relevant components of the key rate calculation. For the purpose of reviewing, we keep this part of discussion general. We direct readers to Refs. [21, 22] for the derivation of the key rate optimization problem and specifically to both Ref. [22] and Appendix A for the technical details regarding the framework of handling the postprocessing

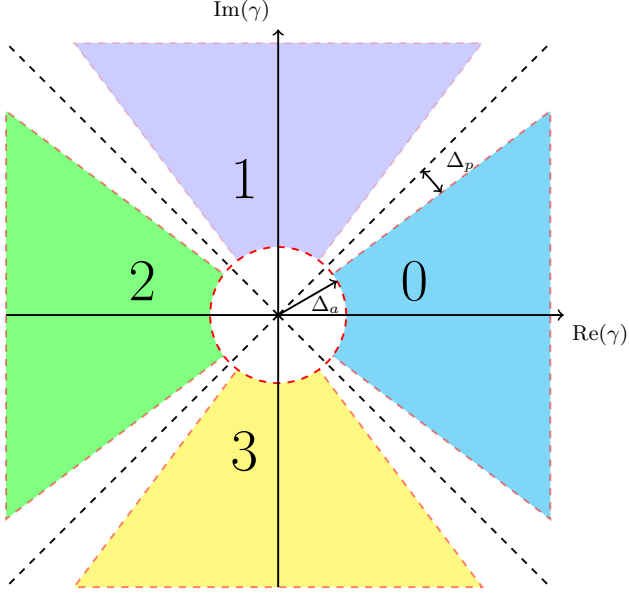


FIG. 1. Key map for protocol 2. When Bob has a measurement outcome $\gamma \in \mathbb{C}$, if γ is in one of the four shaded areas, then Bob maps the measurement outcome to the corresponding value of that area for his key string. If γ is not in the shaded areas, Bob obtains the symbol \perp . Δ_a and Δ_p are two parameters related to postselection.

steps of the protocol. We then briefly discuss the photon number cutoff assumption. Finally, we present the specific numerical optimization problems for these two protocols considered in this work.

A. Numerical method background

We first review the source-replacement scheme, which allows us to recast a prepare-and-measure protocol into an entanglement-based protocol. In the asymptotic limit and under collective attacks, the key rate formula is given by the well-known Devetak-Winter formula [24]. We then briefly discuss how to reformulate Devetak-Winter formula to obtain the relevant convex objective function for the numerical optimization. Finally, we discuss the feasible set of our optimization problem.

1. Source-replacement scheme

Both protocols presented in Sec. II are prepare-and-measure schemes. When we prove the security of a prepare-and-measure scheme, we apply the source-replacement scheme [25, 26] to obtain an equivalent entanglement-based scheme and prove the security of the entanglement-based scheme, which is easier to analyze. The key rate that we obtain from this entanglement-based scheme is also the key rate for the corresponding prepare-and-measure scheme.

If Alice prepares states from the ensemble $\{|\varphi_x\rangle, p_x\}$ in the prepare-and-measure scheme, by the source-replacement scheme, Alice effectively prepares the following bipartite state in the entanglement-based scheme:

$$|\Psi\rangle_{AA'} = \sum_x \sqrt{p_x} |x\rangle_A |\varphi_x\rangle_{A'}, \quad (6)$$

where Alice keeps the register A and sends A' to Bob via a quantum channel. For both protocols considered in this work, $\{|\varphi_x\rangle\} = \{|\alpha\rangle, |-\alpha\rangle, |i\alpha\rangle, |-i\alpha\rangle\}$. To determine which state she sends to Bob, Alice performs a local measurement described by a POVM $M_A = \{M_A^x = |x\rangle\langle x|\}$ on the register A . Upon obtaining a measurement result x , Alice effectively sends to Bob the state $|\varphi_x\rangle$. After the signal in register A' is transmitted via the quantum channel, which is described by a completely positive and trace preserving (CPTP) map $\mathcal{E}_{A' \rightarrow B}$, the bipartite state ρ_{AB} is obtained as

$$\rho_{AB} = (\mathbb{1}_A \otimes \mathcal{E}_{A' \rightarrow B})(|\Psi\rangle\langle\Psi|_{AA'}). \quad (7)$$

Bob then performs a measurement on the register B to obtain his measurement result. When Alice performs a projective measurement $|x\rangle\langle x|$, the corresponding conditional state ρ_B^x that Bob receives is defined as

$$\rho_B^x = \frac{1}{p_x} \text{Tr}_A[\rho_{AB}(|x\rangle\langle x|_A \otimes \mathbb{1}_B)]. \quad (8)$$

2. Key rate formula

The secret key rate under collective attacks in the asymptotic limit is given by the well-known Devetak-Winter formula [24]. In the case of reverse reconciliation [5, 27], this formula reads

$$R^\infty = p_{\text{pass}} \left(I(\mathbf{X}; \mathbf{Z}) - \max_{\rho \in \mathbf{S}} \chi(\mathbf{Z} : E) \right), \quad (9)$$

where $I(\mathbf{X}; \mathbf{Z})$ is the classical mutual information between Alice's string \mathbf{X} and the raw key string \mathbf{Z} , $\chi(\mathbf{Z} : E)$ is the Holevo information that quantifies Eve's knowledge about the raw key string \mathbf{Z} and p_{pass} is the sifting probability, that is, the probability that a given round is used for key generation after the sifting step. The set \mathbf{S} contains all density operators compatible with experimental observations, which we will discuss later. One can rewrite the Devetak-Winter formula as

$$R^\infty = p_{\text{pass}} \left(\min_{\rho \in \mathbf{S}} H(\mathbf{Z}|E) - H(\mathbf{Z}|\mathbf{X}) \right), \quad (10)$$

where $H(\mathbf{Z}|E)$ and $H(\mathbf{Z}|\mathbf{X})$ are conditional von Neumann (Shannon) entropies.

In this formula, $H(\mathbf{Z}|\mathbf{X})$ is amount of information leakage during the error correction step performed at the Shannon limit. In reality, since the error correction cannot be done at the Shannon limit, to take the inefficiency

of error correction into account, we replace this term by the actual amount of information leakage per signal (denoted by δ_{EC}) during the error correction step.

The crucial step to turn this problem into a convex optimization problem is to rewrite $H(\mathbf{Z}|E)$ in terms of Alice and Bob's bipartite quantum state ρ_{AB} . As shown in Refs. [21, 22], the key rate expression can be reformulated as

$$R^\infty = \min_{\rho_{AB} \in \mathbf{S}} D(\mathcal{G}(\rho_{AB}) || \mathcal{Z}(\mathcal{G}(\rho_{AB}))) - p_{\text{pass}} \delta_{EC}. \quad (11)$$

We now explain components in this equation. $D(\rho || \sigma) = \text{Tr}(\rho \log_2 \rho) - \text{Tr}(\rho \log_2 \sigma)$ is the quantum relative entropy. \mathcal{G} is a completely positive and trace non-increasing map. According to Ref. [22], \mathcal{G} describes several classical postprocessing steps of the protocol in terms of actions on the bipartite state ρ_{AB} . Briefly speaking, \mathcal{G} is composed of an announcement map \mathcal{A} , a sifting projection Π and a key map isometry V . The roles are explained as below:

- i) \mathcal{A} is a CPTP map that introduces classical registers \tilde{A} and \tilde{B} to store announcements and also introduces quantum registers \bar{A} and \bar{B} to store measurement outcomes in a coherent fashion (via isometries).
- ii) The sifting projection Π projects the state after announcements to the subspace spanned by announcement outcomes that are kept for the key generation purpose.
- iii) The key map isometry V then utilizes classical announcement registers and quantum measurement outcome registers to perform the key map step described in the protocol and stores the result of key map to a quantum register R .

Thus, $\mathcal{G}(\sigma) = V\Pi\mathcal{A}(\sigma)\Pi V^\dagger$ for an input state σ . We remark that this output state may be subnormalized. The normalization factor is actually p_{pass} . This explains why the factor p_{pass} is not shown in front of the first term in Eq. (11).

Finally, \mathcal{Z} is a pinching quantum channel, which completely dephases the register R to read out the result of key map. If $\{Z_j\}$ is the projective measurement that can be used to obtain the result of key map from the register R , then for an input state σ ,

$$\mathcal{Z}(\sigma) = \sum_j Z_j \sigma Z_j. \quad (12)$$

3. Constraints

We now explain the feasible set \mathbf{S} of our optimization problem. \mathbf{S} is the set of bipartite density operators ρ_{AB} compatible with experimental observations. If $\{\Gamma_i | \Gamma_i = \Gamma_i^\dagger, 1 \leq i \leq M\}$ is the set of experimental observables

for some integer M and $\{\gamma_i \in \mathbb{R} | 1 \leq i \leq M\}$ is the corresponding set of expectation values observed for each Γ_i , then the set \mathbf{S} that we want to optimize over is defined as

$$\mathbf{S} = \{\rho \geq 0 | \text{Tr}(\rho \Gamma_i) = \gamma_i, \forall i\}. \quad (13)$$

In particular, we include the identity operator in the set $\{\Gamma_i\}$ to make sure $\text{Tr}(\rho) = 1$. For a prepare-and-measure scheme, since Eve cannot modify Alice's system A , we additionally require $\rho_A = \text{Tr}_B(\rho_{AB})$ is fixed and given by

$$\rho_A = \sum_{x, x'} \sqrt{p_x p_{x'}} \langle \varphi_{x'} | \varphi_x \rangle |x\rangle \langle x'|_A. \quad (14)$$

A final remark is that this optimization problem is a convex optimization problem and in particular, it is an SDP problem. The objective function here is the quantum relative entropy function whose arguments involve additional linear maps and it is a nonlinear convex function of ρ_{AB} since quantum relative entropy is jointly convex in both arguments. The feasible set is a convex set inside the positive semidefinite cone.

B. Photon number cutoff assumption

The key rate optimization problem in Eq. (11) involves optimizing over all possible bipartite states ρ_{AB} in the feasible set \mathbf{S} . The number of free variables depends on the size of ρ_{AB} . In order to numerically perform the optimization by computer optimization packages, we can only deal with finite-dimensional ρ_{AB} . In our optimization problem, as we can see from the source-replacement scheme, the dimension of Alice's system A is determined by the number of different signal states that she prepares. In both protocols considered in this work, the dimension of the register A is 4. However, since the state that Bob receives is an optical mode and in principle can be manipulated by Eve, Bob's state lives in an infinite-dimensional Hilbert space \mathcal{H}_B . A basis for this Hilbert space is the photon number states $\{|n\rangle : n \in \mathbb{N}\}$. We immediately see that Bob's POVM elements are infinite-dimensional operators and ρ_{AB} is also infinite-dimensional. For DV-QKD, one method to reduce the dimension of the system is to apply a squashing model [28–30] for the protocol to obtain a lower-dimensional representation of his POVM. This is possible for many DV-QKD protocols since one can explicitly formulate the squashing model. However, it is not clear how one can formulate a squashing model for CV systems. Instead, we have to impose an additional assumption in this work in order to perform the numerical optimization. This additional assumption is what we refer as the photon number cutoff assumption. We impose the assumption that Bob's system lives in the Hilbert space $\mathcal{H}_B = \text{span}\{|0\rangle, |1\rangle, \dots, |N_c\rangle\}$ for some cutoff photon number N_c . Namely, if we define

$\Pi_{N_c} = \sum_{n=0}^{N_c} |n\rangle\langle n|$ with a suitable choice of photon number cutoff parameter N_c , we assume $\rho = \Pi_{N_c} \rho \Pi_{N_c}$ for the state ρ under consideration. This photon number cutoff assumption allows us to truncate the infinite-dimensional Hilbert space. If N_c is chosen to be large enough, this assumption is a reasonable working assumption based on the following observations:

- i) Bob can obtain the mean photon number $n_x := \text{Tr}(\rho_B^x \hat{n})$ of each conditional state ρ_B^x via homodyne or heterodyne measurements, where \hat{n} denotes the number operator.
- ii) Since n_x is known, we can pick $N_c \in \mathbb{N}$ such that N_c is much larger than n_x for each $x \in \{0, 1, 2, 3\}$. For such a choice of N_c , the probability of finding the state to have a photon number $n \leq N_c$ is close to 1. This suggests that the contribution from $n > N_c$ photon subspace becomes negligible. Similarly, the off-diagonal blocks $(\mathbb{1} - \Pi_{N_c}) \rho \Pi_{N_c}$ and $\Pi_{N_c} \rho (\mathbb{1} - \Pi_{N_c})$ also have vanishing contributions.
- iii) We can increase N_c to have a numerical verification that the key rate is unchanged after we choose large enough N_c .

This photon number cutoff assumption renders the numerical optimization of the key rate problem feasible. We point out that even though this assumption sounds reasonable, one will have to deliver an exact analysis to remove this assumption for a full security proof. In this sense, our proof is restricted. Nevertheless, we expect the key rates of these protocols will not be affected much by this working assumption. One needs to combine appropriate analytical tools, such as a CV version of the squashing model or a tight error analysis of the key rate due to the photon number cutoff, to reach a complete security proof against collective attacks in the asymptotic limit. Then one needs to apply appropriate tools like quantum de Finetti representation theorem for CV-QKD [31] to reach a full composable security proof [32].

C. Optimization problem for protocol 1 (homodyne detection)

Let \hat{a} and \hat{a}^\dagger be the annihilation and creation operators of a single-mode state, respectively, and they obey the commutation relation $[\hat{a}, \hat{a}^\dagger] = 1$. To be consistent in this work, we define the quadrature operators \hat{q} and \hat{p} as

$$\hat{q} = \frac{1}{\sqrt{2}}(\hat{a}^\dagger + \hat{a}), \quad \hat{p} = \frac{i}{\sqrt{2}}(\hat{a}^\dagger - \hat{a}). \quad (15)$$

They obey the commutation relation $[\hat{q}, \hat{p}] = i$.

From the homodyne measurement, we can obtain expectation values of the first and second moments of the quadrature operators $\langle \hat{q} \rangle$, $\langle \hat{q}^2 \rangle$, $\langle \hat{p} \rangle$ and $\langle \hat{p}^2 \rangle$. We can

calculate the mean photon number of each conditional state ρ_B^x from the homodyne measurement outcomes since $\hat{n} = \frac{1}{2}(\hat{q}^2 + \hat{p}^2 - 1)$. In addition to \hat{n} , we define an operator $\hat{d} = \hat{q}^2 - \hat{p}^2 = \hat{a}^2 + (\hat{a}^\dagger)^2$ to utilize the second moment observations $\langle \hat{q}^2 \rangle$ and $\langle \hat{p}^2 \rangle$ to constrain ρ_{AB} .

The relevant optimization problem is

$$\begin{aligned} & \text{minimize} \quad D(\mathcal{G}(\rho_{AB}) || \mathcal{Z}(\mathcal{G}(\rho_{AB}))) \\ & \text{subject to:} \\ & \quad \text{Tr}[\rho_{AB}(|x\rangle\langle x|_A \otimes \hat{q})] = p_x \langle \hat{q} \rangle_x, \\ & \quad \text{Tr}[\rho_{AB}(|x\rangle\langle x|_A \otimes \hat{p})] = p_x \langle \hat{p} \rangle_x, \\ & \quad \text{Tr}[\rho_{AB}(|x\rangle\langle x|_A \otimes \hat{n})] = p_x \langle \hat{n} \rangle_x, \\ & \quad \text{Tr}[\rho_{AB}(|x\rangle\langle x|_A \otimes \hat{d})] = p_x \langle \hat{d} \rangle_x, \\ & \quad \text{Tr}[\rho_{AB}] = 1, \\ & \quad \text{Tr}_B[\rho_{AB}] = \sum_{i,j=0}^3 \sqrt{p_i p_j} \langle \varphi_j | \varphi_i \rangle |i\rangle\langle j|_A, \\ & \quad \rho_{AB} \geq 0, \end{aligned} \quad (16)$$

where $x \in \{0, 1, 2, 3\}$ and $\langle \hat{q} \rangle_x, \langle \hat{p} \rangle_x, \langle \hat{n} \rangle_x, \langle \hat{d} \rangle_x$ denote the corresponding expectation values of operators $\hat{q}, \hat{p}, \hat{n}, \hat{d}$ for the conditional state ρ_B^x , respectively. In Appendix B, we discuss how we make these operators finite-dimensional under the photon number cutoff assumption.

We remark that one can add more fine-grained constraints using the POVM description of homodyne measurements or using the interval operators I_0, I_1 which we will define shortly. Additional constraints can only improve the key rate as it reduces the size of the feasible set **S**. Nevertheless, we observe that this set of constraints has already given us quite tight key rates. We expect that additional constraints will provide only marginal improvements. For the ease of presentation, we choose this set of coarse-grained constraints.

We now specify the maps \mathcal{G} and \mathcal{Z} . For the reverse reconciliation, the postprocessing map $\mathcal{G}(\sigma) = K\sigma K^\dagger$ is given by the following Kraus operator

$$K = \sum_{z=0}^1 |z\rangle_R \otimes (|0\rangle\langle 0| + |1\rangle\langle 1|)_A \otimes (\sqrt{I_z})_B, \quad (17)$$

where I_0 and I_1 are *interval operators* defined in terms of projections onto (improper) eigenstates of q quadrature:

$$I_0 = \int_{\Delta_c}^{\infty} dq |q\rangle\langle q|, \quad I_1 = \int_{-\infty}^{-\Delta_c} dq |q\rangle\langle q|. \quad (18)$$

In the definition of K , we project Alice's register A onto the subspace spanned by first two basis states (which are related to the states $|\alpha\rangle$ and $|- \alpha\rangle$) and act on Bob's register by interval operators from the q quadrature measurement since we generate keys only when Alice sends $|\alpha\rangle$ or $|- \alpha\rangle$ and when Bob performs q quadrature measurements in this protocol. We remark how the postselection is handled in our security proof. Since Δ_c is a

postselection parameter, the effect of postselection is reflected in the definition of interval operators which are used in the postprocessing map \mathcal{G} . Finally, the pinching quantum channel \mathcal{Z} is described by the projections $Z_0 = |0\rangle\langle 0|_R \otimes \mathbb{1}_{AB}$ and $Z_1 = |1\rangle\langle 1|_R \otimes \mathbb{1}_{AB}$.

We remark that we have made an additional simplification for the Kraus operator K . Unlike the general discussion in Sec. III A or in Ref. [22], we do not introduce the registers $\tilde{A}, \tilde{B}, \bar{A}$ and \bar{B} in the postprocessing map \mathcal{G} for this protocol. The aim of such a simplification is to reduce the total dimension of the quantum states in the key rate optimization without affecting the calculated key rate. We provide a detailed analysis in Appendix A to explain why such a simplification can be made. Here, we discuss the ideas behind this simplification:

- i) The quantum register \bar{A} is Alice's private register that stores her measurement outcome after she performs her POVM $\{M_A^x\}$ on the register A in a coherent fashion. Since Eve has no access to the register \bar{A} , Alice can choose to first perform a coarse-grained measurement that only introduces the announcement register \tilde{A} and then perform a refined measurement conditioned on the announcements, which is described by a local isometry. Moreover, in the reverse reconciliation scheme, since the key map isometry V does not depend on Alice's measurement outcome, the isometry for the refined measurement commutes with both the key map isometry V and the pinching map \mathcal{Z} . As our objective function is invariant under this type of local isometries, we can choose not to apply this isometry and thus, we do not introduce the register \bar{A} .
- ii) In the announcement step, Alice and Bob each announces whether a given round is kept for the key generation. Then the sifting process keeps only one announcement outcome, that is, when they both decide to keep the round. So, both classical registers \tilde{A} and \tilde{B} after applying the sifting projection Π are effectively one-dimensional. We then use another property of the quantum relative entropy regarding quantum-classical states to show that the calculated key rates remain the same if we omit the registers \tilde{A} and \tilde{B} .
- iii) The key map in this protocol only uses the coarse-grained information about Bob's measurement outcomes, that is, in which interval Bob's measurement outcome lies. As with the previous discussion about the register \bar{A} , we can view Bob's measurement in two steps. At the first step, Bob performs a coarse-grained measurement in a coherent fashion to store the desired coarse-grained outcomes in the register \bar{B} . At the second step, Bob performs a refined measurement conditioned on the coarse-grained information to update the register \bar{B} , which is described by a local isometry (denoted by W). Since the key map only uses the coarse-grained information, the key map isometry V effectively needs to first undo the isometry W . So, we can choose not to perform the isometry W and let

the key map isometry V use the coarse-grained information directly. This means the calculated key rate remains the same after we ignore the isometry W . In this case, the key map isometry V simply copies the register \bar{B} to the register R . Thus, we combine these two registers and retain the name of R . The calculated key rate is unaffected because combining two identical registers can be described by an isometry.

D. Optimization problem for protocol 2 (heterodyne detection)

The optimization problem for the protocol 2 has essentially the same form as described in Eq. (16). The differences here are that expectation values are now obtained via the heterodyne detection, and the postprocessing map \mathcal{G} and the pinching map \mathcal{Z} have different forms, as we will present shortly. In principle, we can use additional information about second moments like $\langle \hat{q}\hat{p} \rangle$ to constrain ρ_{AB} as the information becomes available via the heterodyne detection. However, our calculation shows that additional constraints like this can only provide marginal improvements on the key rates in our simulated scenarios. We expect these constraints will be more useful if we introduce squeezing in either the protocol or the simulation.

For an input state ρ , the heterodyne detection gives us the Husimi Q function $Q(\gamma) = \frac{1}{\pi} \langle \gamma | \rho | \gamma \rangle = \text{Tr}(\rho E_\gamma)$, where $\{E_\gamma = \frac{1}{\pi} |\gamma\rangle\langle \gamma| : \gamma \in \mathbb{C}\}$ is the POVM description of the heterodyne measurement. Then from the Q function, we can also obtain values of $\langle \hat{q} \rangle$, $\langle \hat{p} \rangle$, $\langle \hat{n} \rangle$, $\langle \hat{d} \rangle$, whose operators are functions of \hat{a}, \hat{a}^\dagger , by the following equation [33]

$$\text{Tr}[\rho \hat{f}(\hat{a}, \hat{a}^\dagger)] = \langle \hat{f}^{(A)}(\hat{a}, \hat{a}^\dagger) \rangle := \int d^2\gamma Q(\gamma) f^{(A)}(\gamma), \quad (19)$$

where $\hat{f}^{(A)}(\hat{a}, \hat{a}^\dagger)$ is the anti-normal ordered operator of an operator \hat{f} written in terms of \hat{a}, \hat{a}^\dagger , $f^{(A)}(\gamma)$ is the corresponding expression by replacing \hat{a} by γ and \hat{a}^\dagger by γ^* , and $d^2\gamma = d\text{Re}(\gamma)d\text{Im}(\gamma)$.

To write out the Kraus operator for the postprocessing map \mathcal{G} including postselection, we define *region operators* that tell us in which region in Fig. 1 that Bob's measurement outcome lies. We express them using the polar coordinate for the integration as

$$\begin{aligned} R_0 &= \frac{1}{\pi} \int_{\Delta_a}^{\infty} \int_{-\frac{\pi}{4} + \Delta_p}^{\frac{\pi}{4} - \Delta_p} \gamma |\gamma e^{i\theta} \rangle \langle \gamma e^{i\theta}| d\theta d\gamma, \\ R_1 &= \frac{1}{\pi} \int_{\Delta_a}^{\infty} \int_{\frac{\pi}{4} + \Delta_p}^{\frac{3\pi}{4} - \Delta_p} \gamma |\gamma e^{i\theta} \rangle \langle \gamma e^{i\theta}| d\theta d\gamma, \\ R_2 &= \frac{1}{\pi} \int_{\Delta_a}^{\infty} \int_{\frac{3\pi}{4} + \Delta_p}^{\frac{5\pi}{4} - \Delta_p} \gamma |\gamma e^{i\theta} \rangle \langle \gamma e^{i\theta}| d\theta d\gamma, \\ R_3 &= \frac{1}{\pi} \int_{\Delta_a}^{\infty} \int_{\frac{5\pi}{4} + \Delta_p}^{\frac{7\pi}{4} - \Delta_p} \gamma |\gamma e^{i\theta} \rangle \langle \gamma e^{i\theta}| d\theta d\gamma. \end{aligned} \quad (20)$$

The area of integration for each operator corresponds to the relevant region shown in Fig. 1. Again, Δ_a and Δ_p are parameters related to postselection.

In this case, the postprocessing map $\mathcal{G}(\sigma) = K\sigma K^\dagger$ is given by the Kraus operator

$$K = \sum_{z=0}^3 |z\rangle_R \otimes \mathbb{1}_A \otimes (\sqrt{R_z})_B. \quad (21)$$

The pinching quantum channel \mathcal{Z} is given by the projections $Z_j = |j\rangle\langle j|_R \otimes \mathbb{1}_{AB}$ for $j = 0, 1, 2, 3$, that is, for a valid input state σ ,

$$\mathcal{Z}(\sigma) = \sum_{j=0}^3 (|j\rangle\langle j|_R \otimes \mathbb{1}_{AB}) \sigma (|j\rangle\langle j|_R \otimes \mathbb{1}_{AB}). \quad (22)$$

Like protocol 1, we have made a simplification for the Kraus operator K by a similar line of argument.

E. Generalization to other discrete modulation schemes beyond four coherent states

From the description of our security proof method, we remark that this proof technique does not depend on the distribution of the statistics, whether it is Gaussian or not. This is unlike the analytical results presented in Refs. [13, 14]. Also, it is not difficult to see that our method can be generalized to analyze discrete-modulated CV-QKD protocols with more coherent states. If Alice modulates using ℓ coherent states, then Alice's system A is ℓ -dimensional from the source-replacement scheme. In this case, the corresponding optimization problem essentially has the same form as in Eq. (16) except that the index x now runs from 0 to $\ell - 1$ and the maps \mathcal{G} and \mathcal{Z} need to be modified accordingly to match the description of the protocol in a straightforward way. A guide to defining the postprocessing map \mathcal{G} is also provided in Appendix A.

IV. SIMULATION AND KEY RATE

In this section, we first discuss our model for simulating experiments that execute each protocol. From the simulation, we can obtain relevant expectation values like $\langle \hat{q} \rangle, \langle \hat{p} \rangle$ that we usually would obtain from an actual experiment and which are the starting point of our key rate optimization problem as in Eq. (16). Then we comment on the numerical performance of our current algorithm and discuss relevant numerical issues. Finally, we present key rates for both protocols with different variations. We emphasize that our security proof technique of course does not depend on the model of experiment that we use to predict the experimental behavior.

A. Simulation model

To understand how the protocols behave in a realistic scenario, we simulate the quantum channel as a realistic physical channel in the absence of Eve. Such a channel in the context of optical fiber communication can be described by a phase-invariant Gaussian channel with transmittance η and excess noise ξ which is defined as

$$\xi = \frac{(\Delta q_{\text{obs}})^2}{(\Delta q_{\text{vac}})^2} - 1, \quad (23)$$

where $(\Delta q_{\text{vac}})^2$ is the variance of q quadrature for the vacuum state and $(\Delta q_{\text{obs}})^2$ is the variance of q quadrature observed for the signal state. Here we consider the case where both q and p quadratures have the same variance. With our definition of quadrature operators, $(\Delta q_{\text{vac}})^2 = \frac{1}{2}$. In the literature, the value of excess noise is usually reported in a couple of different ways, depending on who makes the observation of $(\Delta q_{\text{obs}})^2$. To avoid possible confusions when discussing the value of excess noise, we clarify these definitions. We use ξ to mean the excess noise in the case where Alice measures $(\Delta q_{\text{obs}})^2$ at the output of her lab and use δ in the case where Bob measures $(\Delta q_{\text{obs}})^2$ for the received signal state.

A natural way to simulate this phase-invariant Gaussian channel is that when Alice prepares a coherent state $|\alpha\rangle$ and sends to Bob via this channel, the output state becomes a displaced thermal state centered at $\sqrt{\eta}\alpha$ with the variance $\frac{1}{2}(1+\delta)$ for each quadrature. An alternative but equivalent way is that when Alice wants to prepare a coherent state $|\alpha\rangle$, the state after preparation becomes a displaced thermal state centered at α with the variance $\frac{1}{2}(1+\xi)$ for each quadrature at the output of her lab. Then the state is transmitted via a pure-loss channel and the final output state that reaches Bob's lab is a displaced thermal state centered at $\sqrt{\eta}\alpha$ with the variance $\frac{1}{2}(1+\eta\xi)$ for each quadrature. Therefore, we see that for this physical channel, $\delta = \eta\xi$. In this work, we use the definition of ξ when we discuss the value of excess noise. Readers should be able to translate between these two definitions by the relation $\delta = \eta\xi$.

Given a displaced thermal state centered at $\sqrt{\eta}\alpha$ with the variance $\frac{1}{2}(1+\eta\xi)$ for each quadrature, we can then calculate our simulated values for $\langle \hat{q} \rangle, \langle \hat{p} \rangle, \langle \hat{n} \rangle$ and $\langle \hat{d} \rangle$ (by either using quasiprobability distribution like Wigner function or Q function of the final state or expanding the final state in the photon number basis). These values can then be supplied to the optimization problem in Eq. (16) which in turn can be solved numerically.

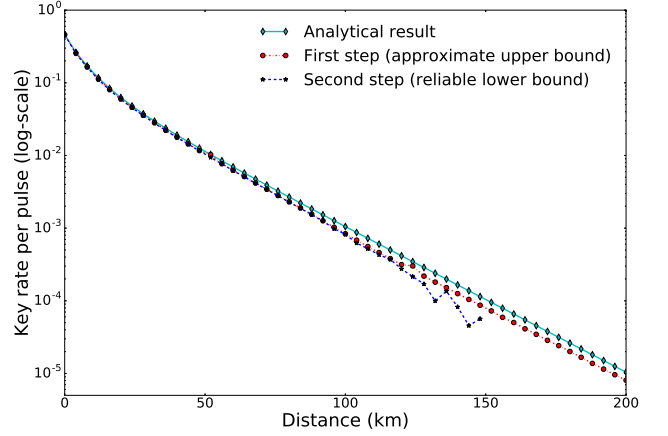
B. About numerical algorithm and performance

To perform the numerical calculation of secret key rates, we apply the two-step procedure mentioned in Ref. [22]. At the first step, we adopt the Frank-Wolfe algorithm [34] to find a sub-optimal attack that gives rise to

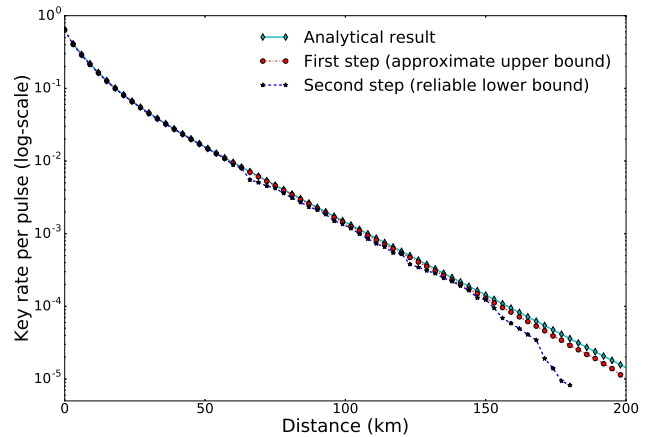
a sub-optimal bipartite state ρ_{AB} . At the second step, we use this sub-optimal ρ_{AB} to solve a linear SDP problem to obtain a reliable lower bound on the key rate, which also takes the constraint violation into consideration. The Frank-Wolfe algorithm used in the first step is an iterative first-order optimization algorithm. We start with an initial choice of ρ_{AB} in the feasible set \mathbf{S} and in each iteration, we solve a linear SDP problem to update the choice of ρ_{AB} until a stopping criterion is satisfied. Since this optimization algorithm may have a very slow rate of convergence near the optimal point in some scenarios, in order to have a reasonable running time, we limit the maximum number of Frank-Wolfe iterations to be 300. To solve linear SDP problems in both first and second steps, we employ the CVX package [35, 36] and SDPT3 [37, 38] solver in MATLAB.

In Fig. 2, we plot the results of the first step and the second step for the protocols 1 and 2 in the case of pure-loss channel ($\xi = 0$) which will be discussed in details in Sec. IV C. Here we utilize this figure to illustrate some aspects of the numerical analysis. The result from the first step can be treated as an approximate upper bound since it is given by a sub-optimal ρ_{AB} . (It is only approximate because the feasible set \mathbf{S} might be enlarged either due to the coarse-graining of constraints or due to the numerical constraint violation.) The result of the second step is a reliable lower bound on the key rate. There are three regions in each plot. Since both plots have similar numerical behaviors, we take Fig. 2a as an example to discuss these three regions. The first region is where both steps give essentially the same results, as we can see for points between 0 km to around 120 km. The second region is between around 120 km to 150 km where there is a noticeable gap between our approximate upper bound and reliable lower bound. This gap is an indicator that the first step algorithm fails to find a good sub-optimal ρ_{AB} . In fact, the chosen number of maximum iterations for the first-step Frank-Wolfe algorithm is reached for those points. The third region is beyond 150 km where the lower bound is missing in the plot. This is because the sub-optimal ρ_{AB} from the first step also has some noticeable constraint violation when the first step terminates prematurely after 300 iterations. Since we take constraint violations into account in the second step calculation to obtain a reliable lower bound according to Ref. [22], these points correspond to the case where the lower bound obtained is zero. To obtain a better lower bound, one needs to improve the result of the first step calculation. There are several possible ways to improve the first step result:

- i) replacing the Frank-Wolfe algorithm by other optimization algorithms;
- ii) using a different SDP solver;
- iii) choosing a different initial point (ρ_{AB}) for the first step;
- iv) increasing the number of iterations.



(a) Protocol 1



(b) Protocol 2

FIG. 2. The key rate versus the transmission distance in the case of pure-loss channel to demonstrate the numerical behavior of the two-step key rate calculation procedure and to compare with the direct evaluation of Devetak-Winter formula (analytical results) for both protocols. The transmittance is modeled as $\eta = 10^{-0.02L}$ for each distance L in km and the reconciliation efficiency is $\beta = 0.95$. The curve with circle marker is the approximate upper bound from the first step and the curve with star marker is the reliable lower bound obtained from the second step. The curve with square marker is the result of direct evaluation via the analytical formula presented in Appendix C without numerical optimization. (a) The key rate for protocol 1 (homodyne detection). The coherent state amplitude α is optimized via a coarse search in the interval $[0.36, 0.6]$. (b) The key rate for protocol 2 (heterodyne detection). The coherent state amplitude α is optimized via a coarse search in the interval $[0.6, 0.95]$.

The main reason behind these alternatives is that different solvers and different algorithms can have different rates of convergence and thus can potentially give better results within the time limit. Since the aim of this work is not about optimizing the numerical optimization algorithm, we choose to report results based on our current choice of algorithm and solver mentioned before with the

limitation of 300 iterations in the first step and we will see that such a choice works well in many scenarios.

For all the remaining figures in this work, we only report the reliable lower bound obtained from the second step. For some of the curves shown in this work, even though there are data points from the second and third scenarios mentioned above, which are not compatible with the general trend of the curve, these numbers can still be safely interpreted as reliable (but very pessimistic) secret key rates. We may expect that if we improve the optimization algorithm (which is not the goal of this work), we can obtain smoother curves. It is also interesting to point out that when we add some nonzero excess noise, the curves that we obtain (shown in later sections) can be smoother than the loss-only curves. We can understand this behavior from the fact that the rank of the density matrix ρ_{AB} is much smaller than its dimension for the loss-only case and thus the problem is not numerically well-conditioned. One can improve on this aspect if one can reformulate the problem using a lower-dimensional representation.

C. Loss-only scenario: comparison to analytical results

We first present the results for the loss-only scenario, that is, $\xi = 0$. For this scenario, we can also obtain an analytical result to have a direct comparison with our numerical result. A direct evaluation of Devetak-Winter formula is possible in this scenario since we can determine relevant Eve's conditional states (up to irrelevant unitaries). As shown in Ref. [20], in the loss-only case, we only need to consider the generalized beam-splitting attack. When Alice sends $|\alpha_x\rangle_{A'}$ to Bob, the state becomes $|\sqrt{\eta}\alpha_x\rangle_B |\sqrt{1-\eta}\alpha_x\rangle_E$ after the pure-loss channel. Eve's conditional states conditioned on Alice's string value x and Bob's raw key string value z effectively live in a two-dimensional subspace for protocol 1 and a four-dimensional subspace for protocol 2. This makes the direct analytical evaluation possible. We leave the procedure of this analytical evaluation to Appendix C. For the numerical key rate optimization, the loss-only scenario follows as a special case of the noisy scenario (using $\xi = 0$) which we discuss in the later sections.

A pure-loss channel is characterized by its transmittance $\eta = 10^{-\frac{\alpha_{\text{att}} L}{10}}$ for each distance L in km with the attenuation coefficient α_{att} , which is 0.2 dB/km for the relevant communication fiber. One may take the quantum efficiency of realistic homodyne/heterodyne detectors into account. A simple but pessimistic way to deal with the detector efficiency is that the loss due to the imperfect detector is also attributed to Eve. In such a worse-case scenario, we can define the total transmittance as $\eta = \eta_{\text{det}} 10^{-0.02L}$, where η_{det} is the quantum efficiency of the detectors. If one defines an effective distance L_0 for the detector inefficiency, that is, $\eta_{\text{det}} = 10^{-0.02L_0}$, then L_0 is less than 13 km for practical homodyne and

heterodyne detectors with the quantum efficiency $\geq 55\%$ [39]. For the ease of presentation and convenience of comparison with other works using different values of detector efficiency, we set $\eta_{\text{det}} = 1$ in this work unless noted otherwise. One may obtain the key rate value corresponding to a realistic value of efficiency by subtracting the effective distance L_0 from all relevant figures.

We plot the key rate versus transmission distance in the loss-only scenario for protocol 1 in Fig. 2a and for protocol 2 in Fig. 2b. For both protocols, we plot both the numerical key rate calculation results and the key rate that can be obtained by a direct evaluation of Devetak-Winter formula. Interestingly, we see that our numerical results are close to the analytical results for both protocols up to the distance around 120 km. Above 120 km, we notice there is a visible gap between our approximate upper bound and reliable lower bound, which indicates there is a room for improvements on the numerical algorithm. We also notice our first step result is slightly lower than the analytical result. The reason is that by analytical analysis, we know the feasible set \mathbf{S} effectively should contain only one state (up to irrelevant unitaries from the perspective of entropy evaluation). However, we use coarse-grained constraints in our numerical optimization and thus the feasible set \mathbf{S} is actually enlarged. We expect that if all fine-grained constraints are used, we should be able to reproduce the analytical results in this loss-only scenario (when a better optimization algorithm is used).

D. Noisy scenario: protocol 1

1. Simulated statistics and error correction cost

We now consider the noisy scenario with nonzero excess noise ξ . From the homodyne measurement, for each $\alpha_x \in \{\alpha, -\alpha, i\alpha, -i\alpha\}$, the simulated statistics is given as

$$\begin{aligned} \langle \hat{q} \rangle_x &= \sqrt{2\eta} \text{Re}(\alpha_x), \\ \langle \hat{p} \rangle_x &= \sqrt{2\eta} \text{Im}(\alpha_x), \\ \langle \hat{n} \rangle_x &= \eta |\alpha_x|^2 + \frac{\eta \xi}{2}, \\ \langle \hat{d} \rangle_x &= \eta (\alpha_x^2 + (\alpha_x^*)^2). \end{aligned} \tag{24}$$

With these values specified, we perform the optimization to bound Eve's information.

Since we simulate the experimental behavior and the cost of error correction is not a part of the optimization, we now present the analytical formula to estimate δ_{EC} from the simulated statistics and numerically evaluate the formula. In this protocol, we only use $|+\alpha\rangle, |-\alpha\rangle$ ($\alpha \in \mathbb{R}$) and the q quadrature measurement to generate keys. After Bob performs his key map, Alice and Bob effectively communicate via a binary channel for the purpose of error correction. From the simulation, the

probability distributions of Bob's q quadrature measurement outcomes for conditional states ρ_B^0 and ρ_B^1 are

$$\begin{aligned} P(q|0) &= \frac{1}{\sqrt{\pi(\eta\xi+1)}} e^{-\frac{(q-\sqrt{2\eta}\alpha)^2}{\eta\xi+1}}, \\ P(q|1) &= \frac{1}{\sqrt{\pi(\eta\xi+1)}} e^{-\frac{(q+\sqrt{2\eta}\alpha)^2}{\eta\xi+1}}. \end{aligned} \quad (25)$$

Since we allow postselection with the cutoff parameter Δ_c , the sifting probability reads

$$\begin{aligned} p_{\text{pass}} &= \frac{1}{2} \left(1 - \int_{-\Delta_c}^{\Delta_c} P(q|0) dq \right) + \frac{1}{2} \left(1 - \int_{-\Delta_c}^{\Delta_c} P(q|1) dq \right) \\ &= 1 - \frac{1}{2} \int_{-\Delta_c}^{\Delta_c} P(q|0) dq - \frac{1}{2} \int_{-\Delta_c}^{\Delta_c} P(q|1) dq. \end{aligned} \quad (26)$$

The error probability between Alice's and Bob's strings is

$$e = \frac{1}{p_{\text{pass}}} \left(\frac{1}{2} \int_{-\Delta_c}^{\Delta_c} P(q|0) dq + \frac{1}{2} \int_{\Delta_c}^{\infty} P(q|1) dq \right). \quad (27)$$

For the error correction performed at the Shannon limit, we have $\delta_{\text{EC}} = H(\mathbf{Z}|\mathbf{X}) = h(e)$, where $h(x) = -x \log_2(x) - (1-x) \log_2(1-x)$ is the binary entropy function. To take into account of the inefficiency of error correction, we first write $\delta_{\text{EC}} = H(\mathbf{Z}|\mathbf{X}) = H(\mathbf{Z}) - I(\mathbf{X}; \mathbf{Z})$ in terms of $I(\mathbf{X}; \mathbf{Z})$ and then scale $I(\mathbf{X}; \mathbf{Z})$ to be $\beta I(\mathbf{X}; \mathbf{Z})$ where β is the reconciliation efficiency whose value is usually reported in CV-QKD literature. Therefore,

$$\begin{aligned} \delta_{\text{EC}} &= H(\mathbf{Z}) - \beta I(\mathbf{X}; \mathbf{Z}) \\ &= (1 - \beta) H(\mathbf{Z}) + \beta H(\mathbf{Z}|\mathbf{X}) \\ &= (1 - \beta) H(\mathbf{Z}) + \beta h(e). \end{aligned} \quad (28)$$

In this work, we use $\beta = 0.95$ in all figures unless mentioned otherwise.

2. Key rates for protocol 1

We first investigate the optimal choice of coherent state amplitude α in the absence of postselection, that is, $\Delta_c = 0$. In Fig. 3, we plot the key rate versus the choice of α for a selected set of distances in the case of the excess noise $\xi = 0.01$. The optimal choice of α for each distance $L = 20, 50, 80, 100$ km lies around 0.4, corresponding to a mean photon number of 0.16 from Alice's source. We also see that the optimal choice does not change significantly for different distances. This observation allows us to search in a restricted interval when we optimize α to maximize the key rate for each transmission distance.

In Fig. 4, we show the secret key rates as a function of the transmission distance for the protocol 1 with homodyne detection for different choices of excess noise ξ . For this plot, we optimize the coherent state amplitude α by a coarse search in the interval $[0.35, 0.6]$. As we can

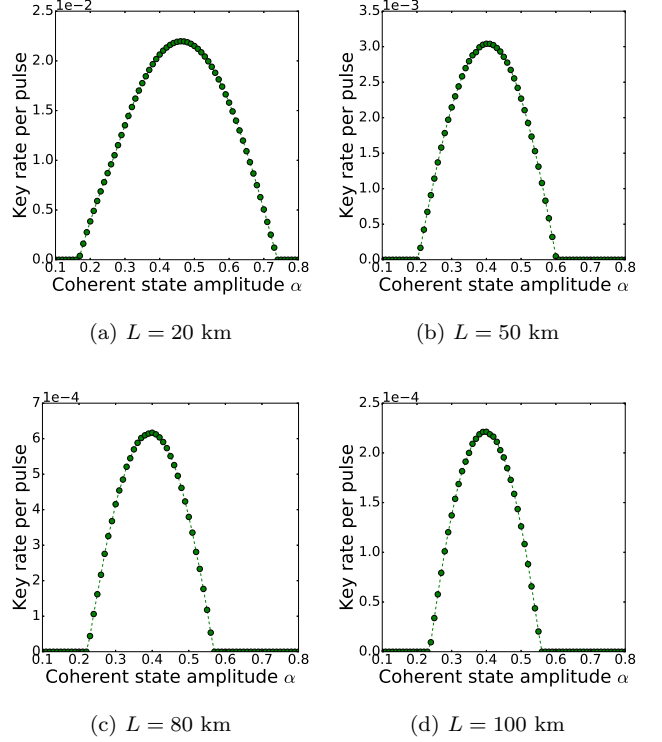


FIG. 3. Secure key rate for protocol 1 versus coherent state amplitude α for a selected choices of distance L . Other parameters: excess noise $\xi = 0.01$ and reconciliation efficiency $\beta = 0.95$.

see from the plot, we can reach around 200 km with experimentally feasible value of excess noise, say, $\xi = 0.01$ [39, 40] with the current technology before the key rate becomes insignificant (say less than 10^{-6} per pulse). To put the number in a more concrete and realistic context, if we consider a system with the repetition rate of 1 GHz and with the detector efficiency 55%, we can obtain 10^3 bits per second at the distance of around 170 km if the total excess noise ξ can be made to be 1% or less.

We also investigate the effects of postselection. The idea of postselection was initially introduced to CV-QKD protocols in order to beat 3 dB limit [18]. The key rate can be potentially improved by discarding very noisy data where Eve has more advantages in determining the raw key than the party (Bob in the case of direct reconciliation and Alice in the case of reverse reconciliation) who needs to match the raw key via the error correction. Intuitively, if we optimize the postselection parameter Δ_c , the key rate can never be lower than the protocol without postselection since one can always set $\Delta_c = 0$ if it is optimal to do so. The important observation here is that our security proof technique allows us to consider postselection with $\Delta_c > 0$ by a simple modification of the post-processing map \mathcal{G} , unlike previous security proofs based on Gaussian optimality. In Fig. 5, we take the case with excess noise $\xi = 0.02$ and the coherent state amplitude

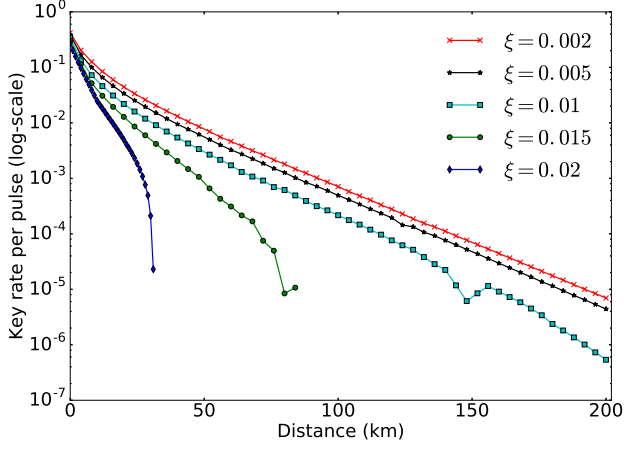


FIG. 4. Secure key rate versus distance for the protocol 1 with homodyne measurement for different values of the excess noise, from top to bottom, $\xi = 0.002, 0.005, 0.01, 0.015, 0.02$. The coherent state amplitude is optimized via a coarse search in the range $[0.35, 0.6]$, the transmittance is $\eta = 10^{-0.02L}$ for each distance L in km and the reconciliation efficiency is $\beta = 0.95$. (See Sec. IV B for an explanation for the non-smoothness of curves.)

$\alpha = 0.45$ as an example to illustrate how the postselection strategy can improve the key rate in the reverse reconciliation scheme and to which extent it can help. We first search an optimal value for the postselection parameter Δ_c by a coarse search and we see in Fig. 5a, the optimal value is around 0.6 at the distance $L = 20$ km. We have also obtained similar plots for different choices of distance and found the optimal value falls roughly in the interval $[0.5, 0.7]$. In Fig. 5b, we compare the key rate with postselection ($\Delta_c > 0$) to that without postselection ($\Delta_c = 0$) for two values of reconciliation efficiency β . In this plot, we optimize the postselection parameter Δ_c via a coarse search in the interval $[0.5, 0.7]$. Since the curves with postselection are above the curves without postselection, we see that the postselection strategy can improve the key rates. We also notice that for reverse reconciliation schemes, the advantage of postselection also depends on the reconciliation efficiency β . The gap between these two scenarios $\Delta_c = 0$ and $\Delta_c > 0$ is smaller when more efficient code (larger β) is used.

E. Noisy scenario: protocol 2

1. Simulated statistics and error correction cost

We now investigate the protocol 2 which uses the heterodyne detection. From the heterodyne measurement, for each conditional state ρ_B^x with $\alpha_x \in \{\alpha, i\alpha, -\alpha, -i\alpha\}$,

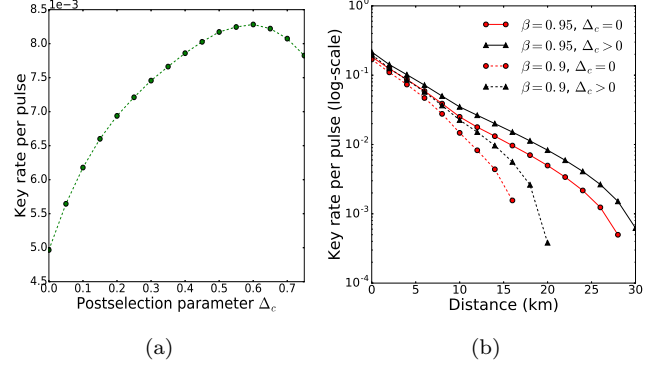


FIG. 5. Secure key rate for the protocol 1 (homodyne detection) with postselection. The excess noise is $\xi = 0.02$ and the coherent state amplitude is $\alpha = 0.45$. (a) Secure key rate versus the postselection parameter Δ_c at the distance $L = 20$ km. The reconciliation efficiency is $\beta = 0.95$. (b) Secure key rate versus the transmission distance with or without postselection for two different values of reconciliation efficiency β . Solid lines have the reconciliation efficiency $\beta = 0.95$ and dashed lines have the reconciliation efficiency $\beta = 0.9$. Lines with (red) circle markers have $\Delta_c = 0$ and lines with (black) triangle markers have Δ_c optimized via a coarse search in the interval $[0.5, 0.7]$. Missing points for the curves reflect that the key rates drop to zero.

we obtain a Q function Q_x as

$$Q_x(\gamma) = \frac{1}{\pi(1 + \eta\xi/2)} \exp\left(-\frac{|\gamma - \sqrt{\eta}\alpha_x|^2}{1 + \eta\xi/2}\right). \quad (29)$$

From each Q function, we can then calculate

$$\begin{aligned} \langle \hat{q} \rangle_x &= \frac{1}{\sqrt{2}} \int (\gamma + \gamma^*) Q_x(\gamma) d^2\gamma = \sqrt{2\eta} \operatorname{Re}(\alpha_x), \\ \langle \hat{p} \rangle_x &= \frac{i}{\sqrt{2}} \int (\gamma^* - \gamma) Q_x(\gamma) d^2\gamma = \sqrt{2\eta} \operatorname{Im}(\alpha_x), \\ \langle \hat{n} \rangle_x &= \int (|\gamma|^2 - 1) Q_x(\gamma) d^2\gamma = \eta|\alpha_x|^2 + \frac{\eta\xi}{2}, \\ \langle \hat{d} \rangle_x &= \int (\gamma^2 + (\gamma^*)^2) Q_x(\gamma) d^2\gamma = \eta(\alpha_x^2 + (\alpha_x^*)^2). \end{aligned} \quad (30)$$

Note those values are exactly the same as from the homodyne measurements since we have the same state after the simulated quantum channel. We obtain those values here indirectly via the Q function.

We also present the procedure to calculate δ_{EC} for protocol 2. We can numerically evaluate $H(\mathbf{Z}|\mathbf{X})$ via the probability distribution:

$$\begin{aligned} P(z = j|x = k) &= \operatorname{Tr}(R_j \rho_B^k) \\ &= \int_{\Delta_a}^{\infty} \int_{\frac{2j-1}{4\pi} + \Delta_p}^{\frac{2j+1}{4\pi} - \Delta_p} \frac{\exp\left(-\frac{|\gamma e^{i\theta} - \sqrt{\eta}\alpha_k|^2}{1 + \eta\xi/2}\right)}{\pi(1 + \eta\xi/2)} \gamma d\theta d\gamma, \end{aligned} \quad (31)$$

where $j, k \in \{0, 1, 2, 3\}$, R_j 's are the region operators defined in Eq. (20) and the conditional state ρ_B^k is defined

in Eq. (8). (In the case of postselection, we then renormalize this probability distribution by the probability of being postselected.) Then δ_{EC} can be calculated by the second line of Eq. (28) as we now take into account that we have an alphabet of four symbols on both sides in the error correction step.

2. Key rates for protocol 2

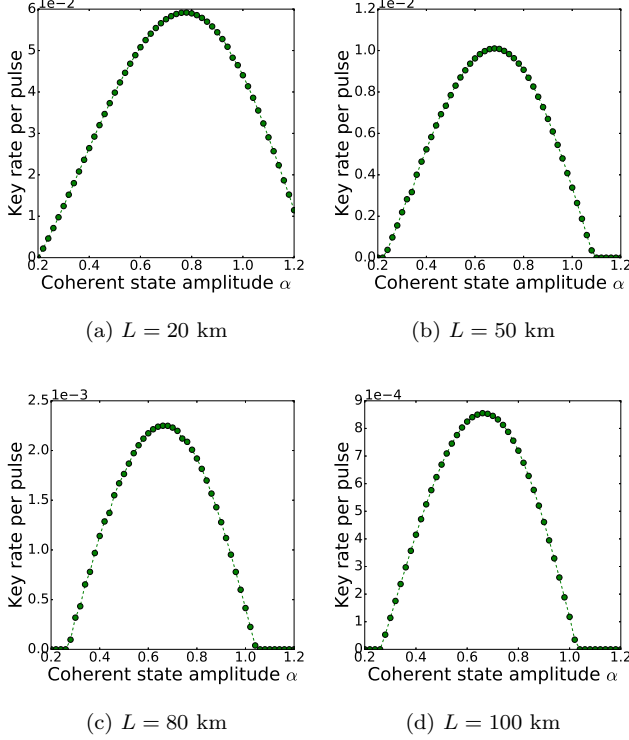


FIG. 6. Secure key rate for protocol 2 versus coherent state amplitude α for selected distances L . Other parameters: excess noise $\xi = 0.01$ and reconciliation efficiency $\beta = 0.95$.

As with the case of protocol 1, we start by investigating the optimal choice of coherent state amplitude α for protocol 2. In Fig. 6, we plot the key rates versus α for selected distances when the excess noise ξ is 0.01. Comparing to Fig. 3, we see that the optimal α for this variant with heterodyne detection is in general larger than that for protocol 1. The optimal choice of α in the protocol 2 is around 0.7 for those selected distances, corresponding to a mean photon number around 0.49, while the optimal choice of α in the protocol 1 is around 0.4 for those selected distances, corresponding to a mean photon number around 0.16. Like the protocol 1, we observe that the optimal value of α for the protocol 2 does not change significantly for a wide range of distances. From the observation here, we later limit our search for optimal choice of α in a restricted interval.

In Fig. 7, we plot the secure key rate versus the trans-

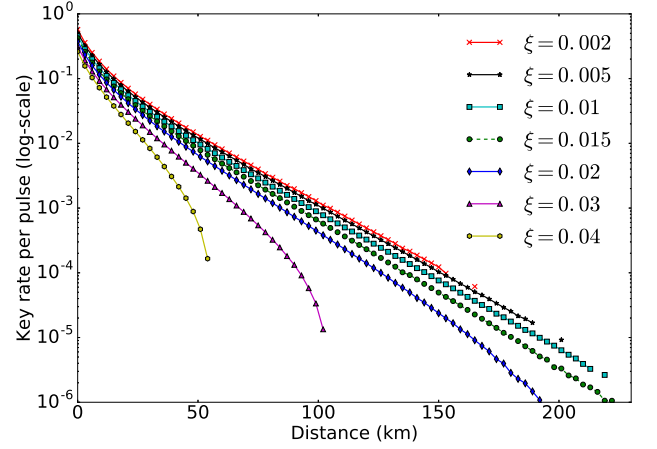


FIG. 7. Secure key rate versus the transmission distance for the protocol 2 with heterodyne detection for different values of the excess noise ξ , from top to bottom, $\xi = 0.002, 0.005, 0.01, 0.015, 0.02, 0.03, 0.04$. The coherent state amplitude is optimized via a coarse search over the interval $[0.6, 0.92]$, the transmittance is $\eta = 10^{-0.02L}$ for each distance L in km and the reconciliation efficiency is $\beta = 0.95$.

mission distance for different values of excess noise ξ . We optimize the coherent state amplitude α via a coarse search over the interval $[0.6, 0.92]$. Interestingly, we see that the key rate for protocol 2 is much higher than protocol 1 when the excess noise is large. For a direct comparison, we replot key rates of both protocols for the values of excess noise $\xi = 0.01$ and 0.02 from Figs. 4 and 7 in Fig. 8. We observe that the protocol 2 achieves much higher key rates and reaches longer distances than the protocol 1 for the same amount of excess noise. In this figure, we also plot the key rate of protocol 2 with the excess noise $\xi = 0.04$ for a direct comparison to the key rate of protocol 1 with the excess noise $\xi = 0.02$. We see that the protocol 2 behaves similarly as the protocol 1 with half of the excess noise for those values of excess noise considered here.

We then compare our results with the security analysis in Ref. [17] for a similar protocol. We differ from that protocol by how the error correction is done, which affects the calculation of the error correction cost term δ_{EC} . In particular, our error correction cost is higher because we discretize Bob's measurement results and only consider binary or quaternary error correcting codes. In Ref. [17], the mutual information $I(\mathbf{X}; \mathbf{Z})$ is obtained by the channel capacity of binary additive white Gaussian noise channel, which is approximated by the capacity of an additive white Gaussian noise channel

$$I(\mathbf{X}; \mathbf{Z}) \approx \log_2 \left(1 + \frac{2\eta\alpha^2}{2 + \eta\xi} \right). \quad (32)$$

This leads to a smaller value of δ_{EC} by the conversion formula in the first line of Eq. (28). In Fig. 9, we plot the key rate results from both our work and Ref.

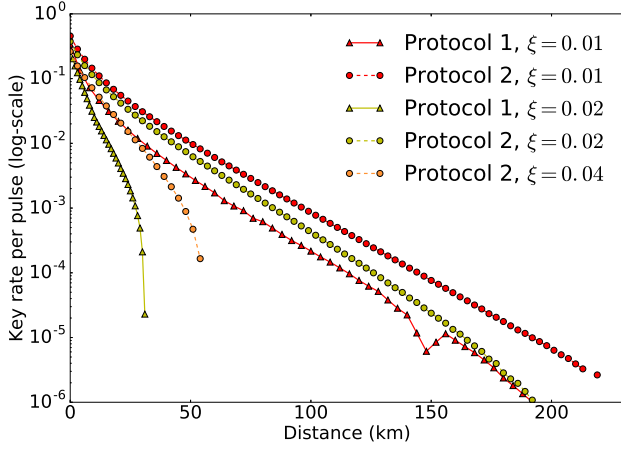


FIG. 8. Secure key rate versus transmission distance for a direct comparison between protocol 1 and protocol 2. Curves for protocol 1 are from Fig. 4 and plotted with triangle markers; the excess noise is $\xi = 0.01, 0.02$ from top to bottom for curves with triangle markers. Curves for protocol 2 are from Fig. 7 and plotted with circle markers; the excess noise is $\xi = 0.01, 0.02, 0.04$ from top to bottom for curves with circle markers.

[17] with a fixed choice of the coherent state amplitude $\alpha = 0.35$ for all distances plotted and with two different values of excess noise. As we can see, our security proof approach provides a remarkable improvement compared with the approach with a reduction to the Gaussian optimality. Our security analysis shows that this protocol has a good tolerance on the excess noise and can extend to significantly longer distances. We emphasize that this choice of $\alpha = 0.35$ is not optimal for both works. While this value is closer to the optimal value found in Ref. [17], the optimal value of the coherent state amplitude found in our work is around 0.7 (for $\xi = 0.01$) as mentioned before. Thus, we also include two curves from Fig. 7 where the coherent state amplitude α is optimized via a coarse search in the interval $[0.6, 0.92]$ for comparisons. As we can see from Fig. 9, the key rate can be significantly improved after we optimize α . We summarize two factors that can boost the key rates. First, our security proof technique gives a tighter estimation of Eve's information compared with the reduction to the Gaussian optimality approach. Second, the key rate can be improved by using a slightly larger value of α than what has been previously investigated. This regime of α was not explored previously because the reduction to the Gaussian optimality approach for discrete modulation schemes gives tight key rates only in the limit of $\alpha \rightarrow 0$ and can give quite loose key rates for large values of α .

Finally, we present the results on the effects of postselection. Our coarse search for values of Δ_p suggests that the optimal value is $\Delta_p = 0$, that is, we do not postselect the data based on the phase. For the postselection parameter Δ_a related to the amplitude of the measured

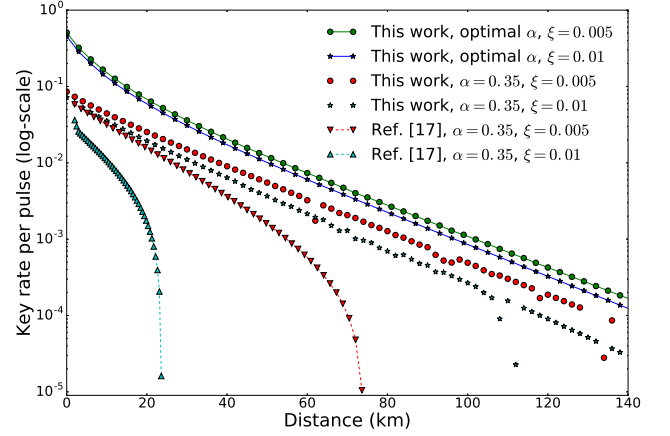


FIG. 9. A comparison of key rates between our work and Ref. [17] for two values of excess noise $\xi = 0.005, 0.01$ and a comparison of key rates between a non-optimal choice of coherent state amplitude α and the optimal choice. Curves with circle and star markers are from this work. Curves with triangle markers are from Ref. [17]. The bottom four curves use a fixed (not optimal) coherent state amplitude $\alpha = 0.35$ and the top two curves optimize the coherent state amplitude. All curves use the reconciliation efficiency $\beta = 0.95$.

complex value from the heterodyne detection, we then perform a coarse search for its optimal value. In Fig. 10, we consider the scenarios with the excess noise $\xi = 0.04$ and with a fixed coherent state amplitude $\alpha = 0.6$ as an example. In Fig. 10a, we plot the key rate versus this parameter Δ_a at the distance $L = 20$ km with the reconciliation efficiency $\beta = 0.95$. From this plot, we observe that the optimal value of Δ_a is around 0.6 at this distance. We have also obtained similar plots for various choices of distance and found that the optimal value roughly falls in the interval $[0.4, 0.7]$. In Fig. 10b, we compare key rates with or without postselection for two different values of reconciliation efficiency at different transmission distances and for this plot, we optimize the values of Δ_a via a coarse search in the interval $[0.4, 0.7]$. We again notice that postselection with reverse reconciliation can improve the key rates. We remark the improvement due to postselection in the reverse reconciliation scheme is more visible for less efficient error-correcting codes, larger excess noise and longer transmission distances. This agrees with the observation made in Ref. [20] under a restricted class of attacks.

V. SUMMARY & OUTLOOK

By numerically solving the key rate optimization problem, we obtain the asymptotic key rates against collective attacks for discrete-modulated CV-QKD protocols with four coherent states and with homodyne or heterodyne detections. We observe that CV-QKD with quadrature phase-shift keying modulation and reverse reconciliation

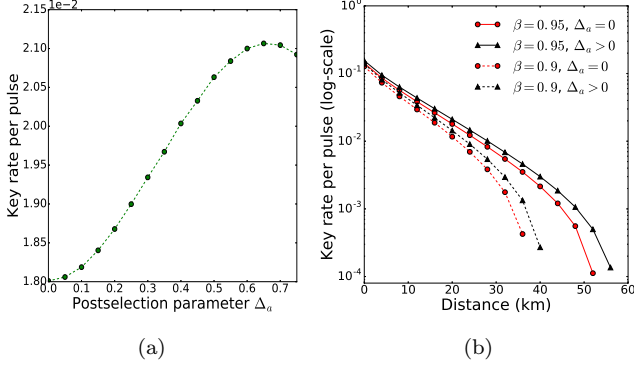


FIG. 10. Secure key rate for the protocol 2 (heterodyne detection) with postselection. The excess noise is $\xi = 0.04$, the coherent state amplitude is $\alpha = 0.6$ and one of postselection parameters is $\Delta_p = 0$. (a) Secure key rate versus the postselection parameter Δ_a at the distance $L = 20$ km. The reconciliation efficiency is $\beta = 0.95$. (b) Secure key rate versus the transmission distance with or without postselection for two different values of reconciliation efficiency β . Solid lines have $\beta = 0.95$ and dashed lines have $\beta = 0.9$. Lines with (red) circle markers have $\Delta_a = 0$ and lines with (black) triangle markers have Δ_a optimized via a coarse search in the interval $[0.4, 0.7]$. Missing points for the curves reflect that the key rates drop to zero.

can significantly improve the key rate compared with previous binary and ternary modulation schemes [13, 14]. Also from the comparison with the results in Ref. [17], we see that our work significantly improves the key rates. Since our security proof approach can give tight key rates, we also see that our key rates can be higher than the one with a linear bosonic channel assumption [15] as the analysis in Ref. [15] is not known to be tight. Thus, our results show that this protocol can achieve comparable key rates as Gaussian modulation schemes. In addition, we consider the effects of postselection and demonstrate that postselection can improve the key rates. Our security analysis imposes a photon number cutoff assumption which truncates the total dimension of system by ignoring the subspace that has negligible contributions. There are multiple paths to remove the photon number cutoff assumption: we either generalize the idea of squashing model to CV protocols, or analytically bound the error due to the photon number cutoff to obtain a key rate lower bound. Finally, one needs to generalize the proof against collective attacks in the asymptotic regime to a composable security proof including finite-size effects using techniques like exponential de Finetti theorem [31].

We also want to point out that key rates of both protocols can be further improved by a better choice of key map and the error correction strategy. In both protocols, we discretize Bob's measurement outcomes to obtain binary or quaternary strings. Therefore, we only consider binary or quaternary error-correcting codes. For a better choice of key map, we may run the optimization in Eq.

(16) with modified \mathcal{G} and \mathcal{Z} maps.

Finally, we comment on how to deal with imperfect detectors. We currently treat detectors as perfect detectors. We can obtain key rates with imperfect detectors by a simple but pessimistic treatment, that is, additional loss and additional excess noise due to imperfect detectors are attributed to Eve. By doing so, we can simply modify two parameters η and ξ to obtain key rates related to imperfect detectors. One may improve the key rates by not giving Eve this additional power and by modeling the imperfection in the POVM description of detectors. We leave further improvements to the future work.

ACKNOWLEDGMENTS

We thank Patrick Coles and Adam Winick for helpful discussions about the numerical method in Ref. [22] and their contributions to the MATLAB codes associated with Ref. [22] and thank Ian George for code review. We thank Anthony Leverrier for helpful discussions and comments on an early version of this manuscript and also for providing data points from Ref. [17] which are used in Fig. 9 for comparison. We thank Christoph Marquardt and Kevin Jaksch for discussion about feasible experimental parameters. The work has been performed at the Institute for Quantum Computing, University of Waterloo, which is supported by Industry Canada. The research has been supported by NSERC under the Discovery Program, Grant No. 341495, and under the Collaborative Research and Development program, Grant No. CRDP J 522308-17. Financial support for this work has been partially provided by Huawei Technologies Canada Co., Ltd.

Appendix A: Framework for postprocessing - derivation and simplification

In this appendix, we present the derivation of the general postprocessing framework in Ref. [22] and then make several observations to simplify the postprocessing map \mathcal{G} in special cases, which leads to a reduction of the dimensions required in the numerical analysis. Finally, we remark how \mathcal{G} maps are simplified in this work.

We make some definitions to set up the notations. When we write an operator on composite registers, we omit the identity operator on the unspecified registers and may reorder registers for the ease of writing. Moreover, the relevant unspecified registers depend on the context. Let \mathcal{X} denote the set of Alice's measurement outcomes. By Alice's announcements S^A , we partition the set \mathcal{X} into subsets \mathcal{X}_a for $a \in S^A$ such that $\mathcal{X} = \bigcup_{a \in S^A} \mathcal{X}_a$. Similarly, we partition Bob's measurement outcomes \mathcal{Y} as $\mathcal{Y} = \bigcup_{b \in S^B} \mathcal{Y}_b$ by his announcements S^B . To simplify our notation, we assume without loss of generality that $|\mathcal{X}_a| = \omega_A$ for all $a \in S^A$ and $|\mathcal{Y}_b| = \omega_B$ for all $b \in S^B$ for some numbers ω_A and ω_B independent of

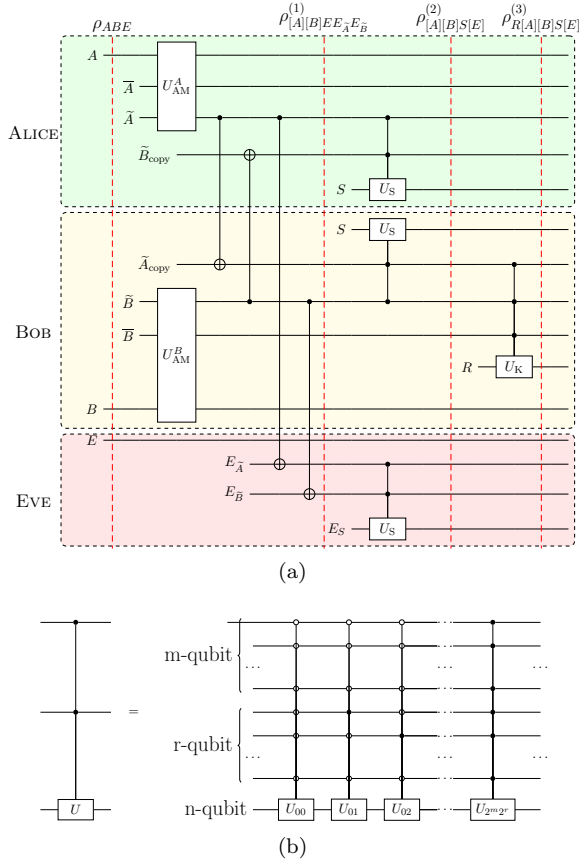


FIG. 11. (a) A schematic circuit diagram for the relevant postprocessing steps: announcement, sifting and key map. Three dashed boxes separate Alice, Bob and Eve's domains. The initial pure state ρ_{ABE} is evolved by an isometry at each step which introduces additional registers and applies a unitary operation on relevant registers. U_{AM}^A, U_{AM}^B, U_S and U_K are unitary operations related to announcement & measurement, sifting and key map. (b) An explanation for the controlled unitary operation used in (a). Here, m, r, n are some sufficiently large integers so that we have a representation of the basis elements for each register in the computational basis of qubits. See text in Appendix A for more explanations.

a and b . This can be easily satisfied by a clever way of book-keeping measurement outcomes. Then, we define a family of maps $f_a : \Omega^A := \{1, 2, \dots, \omega_A\} \rightarrow \mathcal{X}_a$ and a family of maps $f_b : \Omega^B := \{1, 2, \dots, \omega_B\} \rightarrow \mathcal{Y}_b$. Both f_a 's and f_b 's are bijective. Finally, we label Alice's POVM P^A as $P^A := \{P_x^A : x \in \mathcal{X}\} = \{P_{(a, f_a(\alpha))}^A : a \in S^A, \alpha \in \Omega^A\}$ and Bob's POVM $P^B := \{P_y^B : y \in \mathcal{Y}\} = \{P_{(b, f_b(\beta))}^B : b \in S^B, \beta \in \Omega^B\}$.

1. A full model for the relevant postprocessing steps

We give a schematic circuit diagram in Fig. 11 to describe the announcement (including measurement), sifting and key map steps. This diagram covers the scenarios

related to this work and it works for protocols with one round of announcements and with reverse reconciliation. It is not difficult to draw a similar diagram in other scenarios, including the direct reconciliation schemes. Under collective attacks, Alice and Bob share a bipartite quantum state ρ_{AB} after each transmission of quantum signal. In the worst-case scenario, Eve holds a purification ρ_{ABE} of ρ_{AB} . The initial state in the circuit diagram is ρ_{ABE} . At each step, the state is evolved by an isometry, that is, we introduce some local registers and evolve the state by a local unitary. We also keep track of the information leakage during the classical communication. If some information is publicly available during the classical communication in the protocol, then each party holds a copy of the relevant registers. One can recover the classical communication information by measuring a local copy of these registers in the computational basis. Now, we discuss each of the three steps in details.

The isometries related to the announcement and measurement step are denoted by W_A for Alice and W_B for Bob. In particular, W_A first introduces two registers \tilde{A} and \bar{A} , and then applies a unitary operator U_{AM}^A to implement Alice's POVM P^A in a coherent fashion, where announcements are stored in the register \tilde{A} and measurement outcomes are in the register \bar{A} . Like Alice's isometry W_A , Bob's isometry W_B implements his POVM P^B with the announcement register \tilde{B} and measurement outcome register \bar{B} using a local unitary U_{AM}^B . Since the announcement information is available to everyone, Eve obtains a copy (denoted by $E_{\tilde{A}}$) of \tilde{A} and a copy (denoted by $E_{\tilde{B}}$) of \tilde{B} . The coherent version of copying is represented by the controlled NOT operation. Also, Alice and Bob each has a copy of the other party's announcement register, denoted by \tilde{B}_{copy} and \tilde{A}_{copy} respectively. For the convenience of writing, we use \tilde{A} and \tilde{B} to refer to both Alice's and Bob's copies of \tilde{A} and \tilde{B} . As we will see later, we can actually combine the register \tilde{A} with \tilde{A}_{copy} and combine \tilde{B} with \tilde{B}_{copy} in the key rate calculation. In this diagram, the state after the announcement and measurement step is $\rho_{[A][B]EE_{\tilde{A}}E_{\tilde{B}}}^{(1)} = (W_A \otimes W_B) \rho_{ABE} (W_A \otimes W_B)^\dagger$, where for the ease of writing, we reorder the registers and use a shorthand notation for collections of registers: $[A]$ for registers $A\tilde{A}\bar{A}$ and $[B]$ for registers $B\tilde{B}\bar{B}$.

The sifting step partitions the set of announcement events $S^A \times S^B$ as $S^A \times S^B = \mathbf{K} \cup \mathbf{D}$, where \mathbf{K} is the set of announcement events to be kept and \mathbf{D} is the set of announcements to be discarded. The sifting isometry (denoted by V_S) introduces a register S to store the result of sifting (keep or discard) and performs a unitary operator U_S on the local copies of registers \tilde{A} and \tilde{B} to compute the sifting decision. In a common scenario, each party can implement this unitary U_S from the description of a protocol. If it is not from the protocol description and additional classical communication is needed, then after a party implements this unitary operation, other

parties obtain a copy of the register S . For simplicity, we use S to refer to both Alice's and Bob's copies of this register. In the diagram, the state after this sifting step is $\rho_{[A][B]S[E]}^{(2)} = V_S \rho_{[A][B]EE_{\tilde{A}}E_{\tilde{B}}}^{(1)} V_S^\dagger$, where we use a shorthand notation $[E]$ to refer to Eve's collection of registers $EE_{\tilde{A}}E_{\tilde{B}}E_S$.

The key map isometry V_K introduces a register R and applies a local unitary U_K to compute the key map g and to store the result in the register R . This key map g takes the announcement $(a, b) \in S^A \times S^B$ and Alice's measurement outcome $f_a(\alpha)$ in the case of direct reconciliation or Bob's measurement outcome $f_b(\beta)$ in the case of reverse reconciliation as inputs, and outputs a value in $\{0, 1, \dots, N-1\}$ where N is the number of key symbols. For the purpose of derivation, we include an additional key symbol \perp to this set and map all discarded events to it. We will see later that we can eventually remove the symbol \perp from the set of key symbols. In the diagram, the state after the key map state is $\rho_{R[A][B]S[E]}^{(3)} = V_K \rho_{[A][B]S[E]}^{(2)} V_K^\dagger$.

To give explicit expressions for these isometries W_A , W_B , V_S and V_K , we first define K_a^A and K_b^B as

$$\begin{aligned} K_a^A &= \sum_{\alpha \in \Omega^A} \sqrt{P_{(a, f_a(\alpha))}^A} \otimes |a\rangle_{\tilde{A}} \otimes |\alpha\rangle_{\tilde{A}}, \\ K_b^B &= \sum_{\beta \in \Omega^B} \sqrt{P_{(b, f_b(\beta))}^B} \otimes |b\rangle_{\tilde{B}} \otimes |\beta\rangle_{\tilde{B}}, \end{aligned} \quad (\text{A1})$$

where $\{|a\rangle : a \in S^A\}$ and $\{|b\rangle : b \in S^B\}$ are orthonormal bases for registers \tilde{A} ($E_{\tilde{A}}$) and \tilde{B} ($E_{\tilde{B}}$), and $\{|\alpha\rangle : \alpha \in \Omega^A\}$ and $\{|\beta\rangle : \beta \in \Omega^B\}$ are orthonormal bases for registers \tilde{A} and \tilde{B} , respectively. (Note that $|\alpha\rangle$ here is not a coherent state discussed in the main text.) We remark that K_a^A and K_b^B are the same as defined in Eqs. (40) and (41) of Ref. [22] if we write $f_a(\alpha)$ as α_a and $f_b(\beta)$ as β_b . Then W_A , W_B , V_S are defined as

$$\begin{aligned} W_A &= \sum_{a \in S^A} K_a^A \otimes |a\rangle_{E_{\tilde{A}}}, \\ W_B &= \sum_{b \in S^B} K_b^B \otimes |b\rangle_{E_{\tilde{B}}}, \\ V_S &= \Pi \otimes |\mathbf{K}\rangle_S \otimes |\mathbf{K}\rangle_{E_S} + (\mathbb{1}_{\tilde{A}\tilde{B}} - \Pi) \otimes |\mathbf{D}\rangle_S \otimes |\mathbf{D}\rangle_{E_S}, \end{aligned} \quad (\text{A2})$$

where $\Pi = \sum_{(a,b) \in \mathbf{K}} |a\rangle\langle a|_{\tilde{A}} \otimes |b\rangle\langle b|_{\tilde{B}}$ and $\{|\mathbf{K}\rangle, |\mathbf{D}\rangle\}$ is an orthonormal basis for the register S (E_S). To write out the key map isometry V_K , we take the reverse reconciliation schemes as an example and it is straightforward to write out V_K in the case of direct reconciliation schemes by using Alice's measurement outcome $f_a(\alpha)$ instead of Bob's outcome $f_b(\beta)$. We first define an (partial) isometry V on the subspace that Π projects onto and then

write out V_K :

$$\begin{aligned} V &= \sum_{\substack{(a,b) \in \mathbf{K} \\ \beta \in \Omega^B}} |g(a, b, f_b(\beta))\rangle_R \otimes |a\rangle_{\tilde{A}} \otimes |b\rangle_{\tilde{B}} \otimes |\beta\rangle_{\tilde{B}}, \\ V_K &= V\Pi + |\perp\rangle_R \otimes (\mathbb{1}_{\tilde{A}\tilde{B}} - \Pi). \end{aligned} \quad (\text{A3})$$

We remark that the final state $\rho_{R[A][B]S[E]}^{(3)} = V_K V_S (W_A \otimes W_B) \rho_{ABE} (W_A \otimes W_B)^\dagger V_S^\dagger V_K^\dagger$ is a pure state since ρ_{ABE} is a pure state and we only apply isometries to it.

2. Removing the dependence on Eve's registers

To access the key information, we use the projective measurement $\{Z_j = |j\rangle\langle j|_R : j \in \{0, 1, \dots, N-1, \perp\}\}$. Since the final state $\rho_{R[A][B]S[E]}^{(3)}$ is pure, we apply Theorem 1 of Ref. [41] to rewrite conditional entropy $H(\mathbf{Z}|[E])$ as

$$H(\mathbf{Z}|[E]) = D(\rho_{R[A][B]S}^{(3)} \| \sum_j Z_j \rho_{R[A][B]S}^{(3)} Z_j), \quad (\text{A4})$$

where $\rho_{R[A][B]S}^{(3)} = \text{Tr}_{[E]}(\rho_{R[A][B]S[E]}^{(3)})$. We then define an announcement map \mathcal{A} for an input state σ as $\mathcal{A}(\sigma) = \sum_{a \in S^A} \sum_{b \in S^B} (K_a^A \otimes K_b^B) \sigma (K_a^A \otimes K_b^B)^\dagger$ and rewrite $\rho_{R[A][B]S}^{(3)}$ as

$$\begin{aligned} \rho_{R[A][B]S}^{(3)} &= \text{Tr}_{[E]}(\rho_{R[A][B]S[E]}^{(3)}) \\ &= p_{\text{pass}} \rho_{R[A][B]}^{\mathbf{K}} \otimes |\mathbf{K}\rangle\langle \mathbf{K}|_S \\ &\quad + (1 - p_{\text{pass}}) \rho_{R[A][B]}^{\mathbf{D}} \otimes |\mathbf{D}\rangle\langle \mathbf{D}|_S, \end{aligned} \quad (\text{A5})$$

where $p_{\text{pass}} = \text{Tr}(V\Pi\mathcal{A}(\rho_{AB})\Pi V^\dagger) = \text{Tr}(\mathcal{A}(\rho_{AB})\Pi)$ is the same sifting probability defined in the main text and

$$\begin{aligned} \rho_{R[A][B]}^{\mathbf{K}} &= \frac{V\Pi\mathcal{A}(\rho_{AB})\Pi V^\dagger}{p_{\text{pass}}}, \\ \rho_{R[A][B]}^{\mathbf{D}} &= \frac{|\perp\rangle\langle \perp|_R \otimes (\mathbb{1}_{\tilde{A}\tilde{B}} - \Pi) \mathcal{A}(\rho_{AB}) (\mathbb{1}_{\tilde{A}\tilde{B}} - \Pi)}{1 - p_{\text{pass}}}. \end{aligned} \quad (\text{A6})$$

To show that the symbol \perp has no contribution to the key rate, we use the following lemma (see Ref. [42]).

Lemma 1 For quantum-classical states ρ_{QX} and σ_{QX} defined as $\rho_{QX} = \sum_x p(x) \rho_Q^x \otimes |x\rangle\langle x|_X$, $\sigma_{QX} = \sum_x q(x) \sigma_Q^x \otimes |x\rangle\langle x|_X$, where p and q are probability distributions over a finite alphabet \mathcal{X} and ρ_Q^x, σ_Q^x are density operators for all $x \in \mathcal{X}$, the quantum relative entropy is $D(\rho_{QX} \| \sigma_{QX}) = \sum_x p(x) D(\rho_Q^x \| \sigma_Q^x) + D(p \| q)$.

Applying the lemma to the state $\rho_{R[A][B]S}^{(3)}$ with the

classical register S gives us

$$\begin{aligned}
& D(\rho_{R[A][B]S}^{(3)} || \mathcal{Z}(\rho_{R[A][B]S}^{(3)})) \\
&= p_{\text{pass}} D(\rho_{R[A][B]}^{\mathbf{K}} || \mathcal{Z}(\rho_{R[A][B]}^{\mathbf{K}})) \\
&\quad + (1 - p_{\text{pass}}) D(\rho_{R[A][B]}^{\mathbf{D}} || \mathcal{Z}(\rho_{R[A][B]}^{\mathbf{D}})) \quad (\text{A7}) \\
&= p_{\text{pass}} D(\rho_{R[A][B]}^{\mathbf{K}} || \mathcal{Z}(\rho_{R[A][B]}^{\mathbf{K}})) \\
&= D(\mathcal{G}(\rho_{AB}) || \mathcal{Z}(\mathcal{G}(\rho_{AB}))),
\end{aligned}$$

where we define $\mathcal{G}(\rho_{AB}) = V\Pi\mathcal{A}(\rho_{AB})\Pi V^\dagger$, which is the same as in Ref. [22].

Finally, we remark that on the subspace where Π projects, the symbol \perp does not show up anymore. Thus, we can modify $\{Z_j\}$ to remove the symbol \perp in the end. This gives back to the definition of \mathcal{Z} shown in Ref. [22].

3. Simplifying the postprocessing map

We now provide several remarks to explain how we can simplify the map \mathcal{G} while making sure that such a simplification does not change our calculated key rate. Our discussion here takes the reverse reconciliation schemes as an example. It is straightforward to adapt the arguments to the direct reconciliation schemes.

We first make a remark about the registers \tilde{A}_{copy} and \tilde{B}_{copy} that are hidden in our notation \tilde{A} and \tilde{B} . After tracing out Eve's registers $E_{\tilde{A}}$ and $E_{\tilde{B}}$, Alice's register \tilde{A} and Bob's copy \tilde{A}_{copy} are both classical registers and likewise, Bob's register \tilde{B} and Alice's copy \tilde{B}_{copy} are classical. Since each of the sifting and key map steps is done locally via a controlled unitary whose target is the register S or R alone, we can pull out two copies of registers \tilde{A} and \tilde{B} to write the final state in the form of the quantum-classical state to which the previous lemma applies. If we look at the block diagonal structure of $\mathcal{G}(\rho_{AB})$ with respect to two copies of the register \tilde{A} , we see directly that the state with a single copy of the register \tilde{A} is just embedded in a larger space with two copies of the register \tilde{A} . This means the eigenvalues of the state is unaffected by removing one copy of the register \tilde{A} . A similar argument works for two copies of \tilde{B} . Moreover, from the previous lemma, we see immediately that we can calculate the key rate from individual announcements if we write the key map g as $g(a, b, f_b(\beta)) =: g_{ab}(\beta)$ for a collection of functions g_{ab} , one for each $(a, b) \in \mathbf{K}$. In this case, for each $(a, b) \in \mathbf{K}$, we define an isometry $V_{ab} = \sum_{\beta \in \Omega^B} |g_{ab}(\beta)\rangle_R \otimes |\beta\rangle_{\tilde{B}}$ and a completely positive map \mathcal{G}_{ab} for an input state σ as $\mathcal{G}_{ab}(\sigma) = V_{ab}(\tilde{K}_a^A \otimes \tilde{K}_b^B)\sigma(\tilde{K}_a^A \otimes \tilde{K}_b^B)^\dagger V_{ab}^\dagger$, where we define \tilde{K}_a^A such that $K_a^A = \tilde{K}_a^A \otimes |a\rangle_{\tilde{A}}$ and \tilde{K}_b^B such that $K_b^B = \tilde{K}_b^B \otimes |b\rangle_{\tilde{B}}$. Then,

$$\begin{aligned}
& D(\mathcal{G}(\rho_{AB}) || \mathcal{Z}(\mathcal{G}(\rho_{AB}))) \\
&= \sum_{(a,b) \in \mathbf{K}} D(\mathcal{G}_{ab}(\rho_{AB}) || \mathcal{Z}(\mathcal{G}_{ab}(\rho_{AB}))). \quad (\text{A8})
\end{aligned}$$

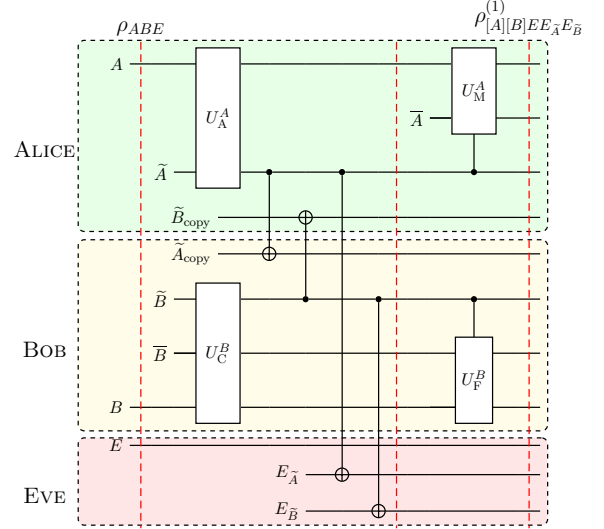


FIG. 12. An alternative description of the announcement step for the reverse reconciliation schemes. This step can be decomposed into two steps. At the first step, Alice only performs a coarse-grained measurement with a unitary U_A^A to obtain announcement results and Bob also performs a coarse-grained measurement with a unitary U_B^B to obtain announcement outcomes and coarse-grained measurement information. At the second step, they choose to perform optional refined measurements (U_M^A and U_F^B) conditioned on the announcements (and previous coarse-grained measurement information for Bob). They can postpone the refined measurements after giving Eve announcement results and in some cases choose not to perform the refined measurements.

Besides the lemma, our objective function has another important property. Since the quantum relative entropy is invariant under an isometry, if an isometry can commute with \mathcal{G} and \mathcal{Z} maps, then our objective function is also invariant under this isometry. In other words, we can add or remove an isometry W (that only acts on Alice's and Bob's registers) in the final expression of Eq. (A7) if W commutes with \mathcal{G} and \mathcal{Z} maps.

From this property of our objective function, if those functions g_{ab} 's are the identity function, then we see that each isometry V_{ab} simply copies the register \tilde{B} and stores this copy to the register R . Removing this copy is a local isometry and renaming the register \tilde{B} by the name R is a unitary. Thus, we can combine the registers \tilde{B} and R and retain the name of R .

Also from this property of our objective function, we now discuss when we can omit the appearance of the register \tilde{A} . As depicted in Fig. 12, the announcement and measurement step can be decomposed into two steps. First, Alice performs a coarse-grained measurement (with associated unitary U_A^A in this figure) to make announcements. Second, conditioned on her own announcement result, Alice performs a refined measurement (with a controlled unitary U_M^A in the figure) if needed to obtain the fine-grained measurement outcomes. As

the refined measurement is done in Alice's local registers to which Eve has no access, Alice's refined measurement can be described by a local isometry. This local isometry can be performed after Eve obtains a copy of the announcement registers. In the reverse reconciliation scheme, since the key map isometry V does not depend on the register \bar{A} , the isometry that describes Alice's refined measurement then commutes with \mathcal{G} and \mathcal{Z} maps. This means that from the key rate calculation perspective, we can drop this isometry due to the property of our objective function. More precisely, if we define $P_a^A = \sum_{\alpha \in \Omega^A} P_{(a, f_a(\alpha))}^A$ for each $a \in S^A$ and define $K_a^{A'} = \sqrt{P_a^A} \otimes |a\rangle_{\bar{A}}$, then we can replace the map \mathcal{G} by the map \mathcal{G}' defined as

$$\mathcal{G}'(\sigma) = V \Pi \left(\sum_{a \in S^A} \sum_{b \in S^B} (K_a^{A'} \otimes K_b) \sigma (K_a^{A'} \otimes K_b^\dagger) \right) \Pi V^\dagger \quad (\text{A9})$$

for an input state σ . (A similar replacement can be done for \mathcal{G}_{ab} .) A similar argument can be applied to the direct reconciliation schemes by interchanging the roles of Alice's and Bob's registers to show that we can omit the register \bar{B} for direct reconciliation.

Along the same line of argument, we remark that the refined measurement conditioned on the announcements can be coarse-grained instead of the fine-grained measurement if the key map only uses the coarse-grained information. This process is also described in Fig. 12. Bob first applies an isometry (with associated unitary U_C^B in the figure) to implement the coarse-grained measurement which gives the same coarse-grained information needed for the key map g and then applies an additional isometry (with associated unitary U_F^B in the figure) to obtain fine-grained measurement outcomes. As the sifting step only depends on the announcement, we can move Bob's refined measurement after the sifting step (not shown in this figure). Since the key map only uses the coarse-grained information, the key map isometry effectively undoes the unitary U_F^B . Therefore, we can take the POVM related to the coarse-grained measurement when we write out Kraus operators K_b^B in Eq. (A1).

Finally, we explain how we derive the Kraus operators shown in Eqs. (17) and (21). First, since we consider the reverse reconciliation schemes, we can omit the measurement outcome register \bar{A} . Second, since the key map of each protocol only uses the coarse-grained measurement outcomes, instead of using Bob's fine-grained POVM corresponding to homodyne or heterodyne measurements, we use the coarse-grained POVM $\{I_0, I_1, 1 - I_0 - I_1\}$ for protocol 1 and $\{R_0, R_1, R_2, R_3, 1 - \sum_{j=0}^3 R_j\}$ for protocol 2). Since the set \mathbf{K} contains only one element, we are left with only one term in the summation of Eq. (A8) after removing registers \bar{A} and \bar{B} . Finally, the key map in this case is the identity map. Thus, we combine registers R and \bar{B} and retain the name R for this combined register.

Appendix B: Operators with photon number cutoff

Let \mathcal{N} denote the photon-number basis up to N_c , that is, $\mathcal{N} = \{|0\rangle, \dots, |N_c\rangle\}$. In this work, we have imposed a photon number cutoff assumption, that is, $\rho_{AB} = (\mathbb{1}_A \otimes \Pi_{N_c}) \rho_{AB} (\mathbb{1}_A \otimes \Pi_{N_c})$ with the projection Π_{N_c} onto the subspace spanned by the basis \mathcal{N} . Since Alice's system is irrelevant for our discussion here, we focus on the conditional states ρ_B^x in the following discussion. For any operator \hat{O} acting on Bob's system, we observe that

$$\begin{aligned} \text{Tr}[\rho_B^x \hat{O}] &= \text{Tr}[\Pi_{N_c} \rho_B^x \Pi_{N_c} \hat{O}] \\ &= \text{Tr}[(\Pi_{N_c} \rho_B^x \Pi_{N_c})(\Pi_{N_c} \hat{O} \Pi_{N_c})]. \end{aligned} \quad (\text{B1})$$

This allows us to define the truncated version of the operator \hat{O} by $\Pi_{N_c} \hat{O} \Pi_{N_c}$. In our optimization problem [see Eq. (16)], the relevant operators are of the forms $\Pi_{N_c} \rho_B^x \Pi_{N_c}$ and $\Pi_{N_c} \hat{O} \Pi_{N_c}$, which have finite-dimensional matrix representations. Specifically, we can find a matrix representation of \hat{O} in the basis \mathcal{N} . We start by writing out the annihilation operator \hat{a} in this basis and then creation operator \hat{a}^\dagger is just its conjugate transpose. Consequently, other relevant operators $\hat{q}, \hat{p}, \hat{n}$ and \hat{d} can be written directly following from their definitions in terms of \hat{a} and \hat{a}^\dagger . In this basis,

$$\Pi_{N_c} \hat{a} \Pi_{N_c} = \begin{pmatrix} 0 & 1 & 0 & 0 & \cdots & 0 \\ 0 & 0 & \sqrt{2} & 0 & \cdots & 0 \\ \vdots & \ddots & & & & \vdots \\ 0 & \cdots & 0 & \sqrt{N_c} & & \\ 0 & \cdots & 0 & 0 & & \end{pmatrix}. \quad (\text{B2})$$

It is not difficult to write out the interval operators I_0, I_1 and region operators R_0, R_1, R_2 and R_3 in this basis. To do so, we use the overlap $\langle q|n\rangle$ between a quadrature eigenstate $|q\rangle$ and a photon-number state $|n\rangle$ and the overlap $\langle \gamma e^{i\theta}|n\rangle$ between a coherent state $|\gamma e^{i\theta}\rangle$ and a photon-number state $|n\rangle$. With our definition of quadrature operators in Eq. (15), the overlaps $\langle q|n\rangle$ and $\langle \gamma e^{i\theta}|n\rangle$ read [43]

$$\begin{aligned} \langle q|n\rangle &= \frac{1}{\sqrt{\pi^{\frac{1}{2}} 2^n (n!)}} \exp\left(-\frac{q^2}{2}\right) H_n(q), \\ \langle \gamma e^{i\theta}|n\rangle &= e^{-\frac{\gamma^2}{2}} \frac{\gamma^n e^{-in\theta}}{\sqrt{n!}}, \end{aligned} \quad (\text{B3})$$

where H_n is the Hermite polynomial of order n . We then perform the relevant integrals to obtain a finite-dimensional matrix representation in this basis.

Finally, in the expression of the Kraus operators shown in Eqs. (17) and (21), we need to take the square root of each of the interval operators I_0, I_1 or region operators R_0, R_1, R_2 and R_3 . Even though these operators are projective on the entire infinite-dimensional space such

that the square root of each operator is itself, the truncated version of each such operator is no longer projective in the finite-dimensional subspace spanned by the basis \mathcal{N} . Thus, a caution about the ordering of truncation and square root is needed. We now explain the proper way to handle this. With the photon number cutoff assumption $\rho = \Pi_{N_c} \rho \Pi_{N_c}$, we see from Eq. (B1) that for a POVM element F on the infinite-dimensional space, the corresponding POVM element on this finite-dimensional subspace becomes $\Pi_{N_c} F \Pi_{N_c}$. As we know from Appendix A, the purpose of taking the square root of a POVM element is to realize this POVM measurement in an isometric fashion. Since the relevant POVM element on this finite-dimensional subspace is $\Pi_{N_c} F \Pi_{N_c}$, we need to take the square root of $\Pi_{N_c} F \Pi_{N_c}$. This means we take the truncation first and then take the square root.

Appendix C: Evaluation of loss-only key rate

We discuss how to evaluate the Devetak-Winter formula in the loss-only scenario in the absence of posts-election. When Alice sends $|\alpha_x\rangle_{A'}$ to Bob, in the absence of noise, Bob can verify that he receives a pure coherent state via homodyne or heterodyne detections. In the case of homodyne detection, Bob can verify that the received state is a minimum uncertainty state with the same variance for both quadratures, which implies it is a pure coherent state. In the case heterodyne detection, Bob performs a tomography to verify that the received state is a pure coherent state. In particular if Bob verifies his state to be an attenuated coherent state $|\sqrt{\eta}\alpha_x\rangle$, it has been shown [20] that Eve's optimal attack is the generalized beamsplitting attack for this pure-loss channel. Thus, the state shared by Bob and Eve becomes $|\sqrt{\eta}\alpha_x\rangle_B |\sqrt{1-\eta}\alpha_x\rangle_E$ after this channel. Due to the product state structure of Bob and Eve's joint state, Bob's measurement outcome does not influence Eve's state. Therefore, conditioned on the value x of Alice's string \mathbf{X} and the value z in Bob's raw key \mathcal{Z} , Eve's conditional state $|\epsilon_{x,z}\rangle$ is

$$|\epsilon_{x,z}\rangle = |\sqrt{1-\eta}\alpha_x\rangle := |\epsilon_x\rangle, \quad (\text{C1})$$

which is independent from z and thus we call it $|\epsilon_x\rangle$ for simplicity.

1. Protocol 1

The procedure outlined here is similar to the calculation in Ref. [20]. For the protocol 1, since $\alpha_x \in \{\alpha, -\alpha\}$, Eve's conditional states $|\epsilon_x\rangle$ are either $|\sqrt{1-\eta}\alpha\rangle$ or $|\sqrt{1-\eta}\alpha\rangle$, which only span a two-dimensional subspace. We can find a two-dimensional representation of

$|\epsilon_x\rangle$ as

$$\begin{aligned} |\epsilon_0\rangle &= |\sqrt{1-\eta}\alpha\rangle = c_0 |e_0\rangle + c_1 |e_1\rangle, \\ |\epsilon_1\rangle &= |-\sqrt{1-\eta}\alpha\rangle = c_0 |e_0\rangle - c_1 |e_1\rangle, \end{aligned} \quad (\text{C2})$$

where $|e_0\rangle, |e_1\rangle$ are defined as

$$\begin{aligned} |e_0\rangle &= \frac{1}{\sqrt{\cosh[(1-\eta)\alpha^2]}} \sum_{n=0}^{\infty} \frac{(\sqrt{1-\eta}\alpha)^{2n}}{\sqrt{(2n)!}} |2n\rangle, \\ |e_1\rangle &= \frac{1}{\sqrt{\sinh[(1-\eta)\alpha^2]}} \sum_{n=0}^{\infty} \frac{(\sqrt{1-\eta}\alpha)^{2n+1}}{\sqrt{(2n+1)!}} |2n+1\rangle, \end{aligned} \quad (\text{C3})$$

and $c_0 = e^{-\frac{(1-\eta)\alpha^2}{2}} \sqrt{\cosh[(1-\eta)\alpha^2]}$ and $c_1 = e^{-\frac{(1-\eta)\alpha^2}{2}} \sqrt{\sinh[(1-\eta)\alpha^2]}$.

We now directly evaluate the Devetak-Winter formula

$$R^\infty = \beta I(\mathbf{X}; \mathbf{Z}) - \chi(\mathbf{Z} : E). \quad (\text{C4})$$

We obtain $I(\mathbf{X}; \mathbf{Z})$ by calculation similar to Eq. (28). We can directly calculate $\chi(\mathbf{Z} : E)$ via

$$\chi(\mathbf{Z} : E) = H(\bar{\rho}_E) - \sum_{j=0}^1 P(z=j) H(\rho_{E,j}), \quad (\text{C5})$$

where $H(\sigma) = -\text{Tr}(\sigma \log_2 \sigma)$ is the von Neumann entropy and the relevant states are

$$\begin{aligned} \rho_{E,j} &= \sum_{i=0}^1 \frac{P(x=i, z=j)}{P(z=j)} |\epsilon_i\rangle\langle\epsilon_i|, \\ \bar{\rho}_E &= \sum_{j=0}^1 P(z=j) \rho_{E,j}, \end{aligned} \quad (\text{C6})$$

where $P(x, z)$ is the joint probability distribution of x and z and $P(z)$ is the marginal probability distribution of z . These relevant Eve's states $|\epsilon_x\rangle$ all have a two-dimensional matrix representation in the basis $\{|e_0\rangle, |e_1\rangle\}$ and thus it is straightforward to directly evaluate the Devetak-Winter formula.

2. Protocol 2

For the protocol 2, since $\alpha_x \in \{\alpha, i\alpha, -\alpha, -i\alpha\}$, Eve's conditional states $|\epsilon_x\rangle$ are $|\sqrt{1-\eta}\alpha\rangle, |i\sqrt{1-\eta}\alpha\rangle, |-\sqrt{1-\eta}\alpha\rangle, |-i\sqrt{1-\eta}\alpha\rangle$, which only span a four-dimensional subspace. Therefore, we can find an orthonormal basis $\{|f_0\rangle, |f_1\rangle, |f_2\rangle, |f_3\rangle\}$ for this subspace similar to the basis $\{|e_0\rangle, |e_1\rangle\}$ and find a four-dimensional matrix presentation for each of Eve's conditional states (see Ref. [44] for an explicit expression). All the procedures are similar to protocol 1 except that the summation indexes i, j now run from 0 to 3 instead of 0 to 1 in Eqs. (C5) and (C6). With a four-dimensional matrix representation of Eve's conditional states $|\epsilon_x\rangle$ in the basis $\{|f_0\rangle, |f_1\rangle, |f_2\rangle, |f_3\rangle\}$, it is also straightforward to directly evaluate the Devetak-Winter formula.

-
- [1] C. H. Bennett and G. Brassard, in *Proceedings of IEEE International Conference on Computers, Systems and Signal Processing* (IEEE, New York, 1984) pp. 175–179.
 - [2] A. K. Ekert, Phys. Rev. Lett. **67**, 661 (1991).
 - [3] V. Scarani, H. Bechmann-Pasquinucci, N. J. Cerf, M. Dušek, N. Lütkenhaus, and M. Peev, Rev. Mod. Phys. **81**, 1301 (2009).
 - [4] F. Grosshans and P. Grangier, Phys. Rev. Lett. **88**, 057902 (2002).
 - [5] F. Grosshans, G. Van Assche, J. Wenger, R. Brouri, N. J. Cerf, and P. Grangier, Nature **421**, 238 (2003).
 - [6] C. Weedbrook, A. M. Lance, W. P. Bowen, T. Symul, T. C. Ralph, and P. K. Lam, Phys. Rev. Lett. **93**, 170504 (2004).
 - [7] M. Navascués, F. Grosshans, and A. Acín, Phys. Rev. Lett. **97**, 190502 (2006).
 - [8] R. García-Patrón and N. J. Cerf, Phys. Rev. Lett. **97**, 190503 (2006).
 - [9] E. Diamanti and A. Leverrier, Entropy **17**, 6072 (2015).
 - [10] P. Jouguet, S. Kunz-Jacques, E. Diamanti, and A. Leverrier, Phys. Rev. A **86**, 032309 (2012).
 - [11] E. Kaur, S. Guha, and M. M. Wilde, “Asymptotic security of discrete-modulation protocols for continuous-variable quantum key distribution,” (2019), arXiv:1901.10099.
 - [12] H. Häselser and N. Lütkenhaus, Physical Review A **81**, 060306 (2010).
 - [13] Y.-B. Zhao, M. Heid, J. Rigas, and N. Lütkenhaus, Phys. Rev. A **79**, 012307 (2009).
 - [14] K. Brádler and C. Weedbrook, Phys. Rev. A **97**, 022310 (2018).
 - [15] A. Leverrier and P. Grangier, Phys. Rev. Lett. **102**, 180504 (2009).
 - [16] T. Hirano, T. Ichikawa, T. Matsubara, M. Ono, Y. Oguri, R. Namiki, K. Kasai, R. Matsumoto, and T. Tsurumaru, Quantum Science and Technology **2**, 024010 (2017).
 - [17] S. Ghorai, P. Grangier, E. Diamanti, and A. Leverrier, “Asymptotic security of continuous-variable quantum key distribution with a discrete modulation,” (2019), arXiv:1902.01317.
 - [18] C. Silberhorn, T. C. Ralph, N. Lütkenhaus, and G. Leuchs, Phys. Rev. Lett. **89**, 167901 (2002).
 - [19] M. Heid and N. Lütkenhaus, Phys. Rev. A **76**, 022313 (2007).
 - [20] M. Heid and N. Lütkenhaus, Physical Review A **73**, 052316 (2006).
 - [21] P. J. Coles, E. M. Metodiev, and N. Lütkenhaus, Nat. Commun. **7**, 11712 (2016).
 - [22] A. Winick, N. Lütkenhaus, and P. J. Coles, Quantum **2**, 77 (2018).
 - [23] H.-K. Lo, H. F. Chau, and M. Ardehali, J. Cryptol. **18**, 133 (2004).
 - [24] I. Devetak and A. Winter, Proc. R. Soc. A **461**, 207 (2005).
 - [25] M. Curty, M. Lewenstein, and N. Lütkenhaus, Phys. Rev. Lett. **92**, 217903 (2004).
 - [26] A. Ferenczi and N. Lütkenhaus, Phys. Rev. A **85**, 052310 (2012).
 - [27] F. Grosshans, N. J. Cerf, J. Wenger, R. Tualle-Brouri, and P. Grangier, Quantum Inf. Comput **3**, 535 (2003).
 - [28] N. J. Beaudry, T. Moroder, and N. Lütkenhaus, Phys. Rev. Lett. **101**, 093601 (2008).
 - [29] T. Tsurumaru, Physical Review A **81**, 012328 (2010).
 - [30] O. Gittsovich, N. J. Beaudry, V. Narasimhachar, R. R. Alvarez, T. Moroder, and N. Lütkenhaus, Phys. Rev. A **89**, 012325 (2014).
 - [31] R. Renner and J. I. Cirac, Phys. Rev. Lett. **102**, 110504 (2009).
 - [32] R. Renner, *Security of Quantum Key Distribution*, Ph.D. thesis, ETH Zürich, Zürich, Switzerland (2005), arXiv:quant-ph/0512258.
 - [33] W. Vogel and D.-G. Welsch, *Quantum optics* (John Wiley & Sons, 2006).
 - [34] M. Frank and P. Wolfe, Naval research logistics quarterly **3**, 95 (1956).
 - [35] CVX Research, Inc., “CVX: Matlab software for disciplined convex programming, version 2.0,” <http://cvxr.com/cvx> (2012).
 - [36] M. Grant and S. Boyd, in *Recent Advances in Learning and Control*, Lecture Notes in Control and Information Sciences, edited by V. Blondel, S. Boyd, and H. Kimura (Springer-Verlag Limited, 2008) pp. 95–110.
 - [37] K. C. Toh, M. J. Todd, and R. H. Tutuncu, Optimization Methods and Software **11**, 545 (1991).
 - [38] R. H. Tutuncu, K. C. Toh, and M. J. Todd, Mathematical Programming Ser. B **95**, 189 (2003).
 - [39] P. Jouguet, S. Kunz-Jacques, A. Leverrier, P. Grangier, and E. Diamanti, Nature photonics **7**, 378 (2013).
 - [40] D. Huang, P. Huang, D. Lin, and G. Zeng, Scientific reports **6**, 19201 (2016).
 - [41] P. J. Coles, Physical Review A **85**, 042103 (2012).
 - [42] M. M. Wilde, *Quantum information theory* (Cambridge University Press, 2013).
 - [43] S. Barnett and P. M. Radmore, *Methods in theoretical quantum optics*, Vol. 15 (Oxford University Press, 2002).
 - [44] M. Dušek, M. Jähma, and N. Lütkenhaus, Physical Review A **62**, 022306 (2000).